A NEW METHODOLOGY FOR DETECTING INCIPIENT FAULTS IN ELECTRIC MACHINERY

by

Pratik Bhogale

A dissertation submitted to the faculty of
The University of North Carolina at Charlotte
in partial fulfillment of the requirements
for the degree of the Master of Science in
Electrical Engineering

Charlotte

2022

Approved by:

_____

Dr. Jeremy Holleman

_____

Dr. Valentina Cecchi

_____

Dr. Robert W. Cox

ABSTRACT

PRATIK BHOGALE. A New Methodology for Detecting Incipient Faults in Electric Machinery. (Under the Direction of DR. ROBERT W. COX)

Faults in electric machinery such as generators, although rare, still costs hundreds of thousands of dollars for diagnostics, repairs along with extra cost incurred by the downtime of the machine. This thesis proposes a new way, which is cheaper in terms of hardware cost, and advantageous in ways like live and visual monitoring, live data collection and feature extraction for fault detection, and portability of apparatus. The proposed methodology uses an edge compute device along with software-defined radio to achieve the goal. The thesis includes discussion for feature extraction from the collected data, which will be used for fault or anomaly detection using machine learning solutions. Signals collected via the neutral ground are used for fault detection, in this approach. The concepts of "partial discharge analysis" and time-series data extraction from the collected data, are focused on primarily.

DEDICATION

To all the engineers who help make the world a better place.

ACKNOWLEDGMENTS

I would like to thank my advisor Dr. Robert Cox. His humility bundled with perspective to look at any problem and explain it in the simplest way possible, made this thesis easier for me. His constant motivation and patience towards me, especially during the times when it would have been completely justified to not be patient or humble or calm has helped me become a better engineer and a better person.

Special thanks to Mr. Paul N. Lesner and Mr. Charles R Sammons Jr. for their constant help and support, letting us use the Duke Energy powerplants for collection and monitoring data for this research. This would not have been possible without them.

I would like thank Dr. Valentina Cecchi and Dr. Jeremy Holleman of this thesis committee for their support and time.

Finally, I would like to thank my parents, my sister, and friends whose love and support help me reach this point.

TABLE OF CONTENTS

LIST OF TABLES

LIST OF FIGURES

CHAPTER 1: INTRODUCTION AND BACKGROUND

Large electric motors and generators are the workhorses of the modern economy. It is thus desirable to prevent major machinery failures that cause significant downtime in plants or factories. When a large generator fails in a nuclear power plant, for instance, the lost revenue can be over $1M per day. When sudden failures occur, plants go offline for days or weeks while repair is completed. Ideally, one would detect such failures at an early stage so that maintenance could be planned and perhaps aligned with pre-planned outages. Detecting early-stage faults requires technologies that can affordably and reliably measure small signals that indicate potential failures. Such signals can come in the form of vibrations, electric currents, or temperatures. This thesis describes a technology that could be used to detect early-stage failures arising from internal failures caused by degraded winding insulation or faulty bearings. The core technology is a software-defined radio (SDR), which is a low-cost device that can measure high frequency, common-mode currents flowing out of the machine. The SDR is paired with a low-cost edge-compute platform to provide a simple device that fits into an internet-of-things (IoT) framework.

1.1 Motivation

The electric power sector is experiencing many changes, and these are prompting a need for new low-cost monitoring techniques. Nuclear plants were initially designed to operate for 20 years but the utilities now have the confidence and data they need for license renewal for 20-40 more years of operation. This not only means that the plants are getting very old but also that they need better monitoring techniques to detect faults before they cause catastrophic damage. Intermittent renewables such as hydropower, natural gas, solar

energy, and wind energy are causing some machines to operate more dynamically by sharing the load. Distributed generations mean there are far more generators located in more remote locations. All these different generators at different remote locations call for the use of remote monitoring techniques for early fault detection. The technique needs to be robust and easy to deploy at remote locations, while also capable to be accessed remotely and get a runtime analysis.

1.2 Proposed Technology

During the 1980s, engineers at American Electric Power (AEP) found that certain early-stage generator and motor faults could be detected by placing small radios next to the machines. Using AM and FM radios, the engineers could hear sounds that could be correlated with certain failures. The technique came to be known as Electromagnetic Signature Analysis (EMSA). During the 1990s, the Electric Power Research Institute (EPRI) formed an EMSA working group consisting of experts from several major utilities. EPRI worked with these utilities to develop a formal framework for implementing EMSA. This approach has been adopted by several large utilities, but it is expensive and not scalable. Chapter 2 provides extensive details on the existing approach.

FIGURE 1.1: Engineer using a handheld EMI sniffer to scan motor to receive AM signals[14].

FIGURE 1.2: Engineer using a handheld EMI sniffer to scan switchgear[14].

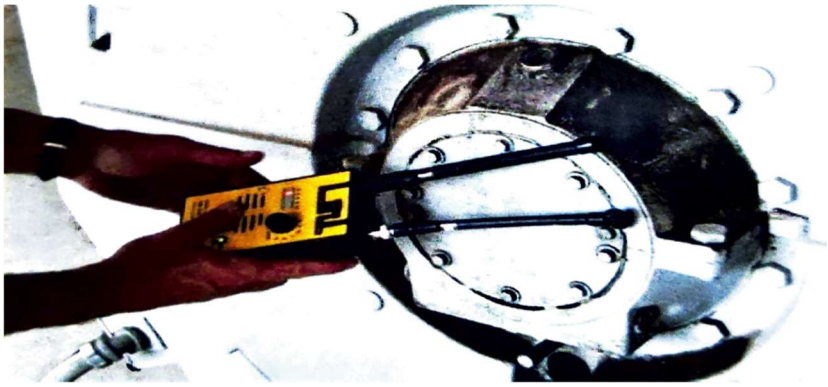

FIGURE 1.3: Engineer using a handheld EMI sniffer to scan bearings[14].

This project began following extensive discussions with utility stakeholders. These conversations quickly revealed a significant limitation with existing technology. Specifically, the earliest users of EMSA described their ability to find faults by listening to radios. These engineers could hear audible patterns attributable to certain early-stage problems. Table 1.1 lists several of the patterns compiled by EPRI. These descriptions are notably ad hoc, but they indicate the existence of patterns. This observation motivates modern engineers to consider opportunities for machine learning (ML) and artificial intelligence (AI). Discussions with utility engineers, however, indicated that current EMSA technology could not capture these patterns. The current technique uses sophisticated, laboratory-grade hardware to replicate the functioning of an AM radio at 8000 different frequencies between 30kHz and 100MHz.[14] The resulting signals could be recorded and listened to on a radio so that one could hear the patterns listed in Table 1.1. Unfortunately, this process results in a large amount of data, so engineers record one summary statistic to describe the average value of the amplitude at each frequency. Using this technique, much of the value of EMSA is lost.

TABLE 1.1: Sound patterns corelating to fault conditions [14]

Sound Pattern	Correlated Fault Condition
Bacon Frying	Corona discharge inside a machine
Distinctive Buzzing	Microsparking
Popping or Rasping	Partial Discharge

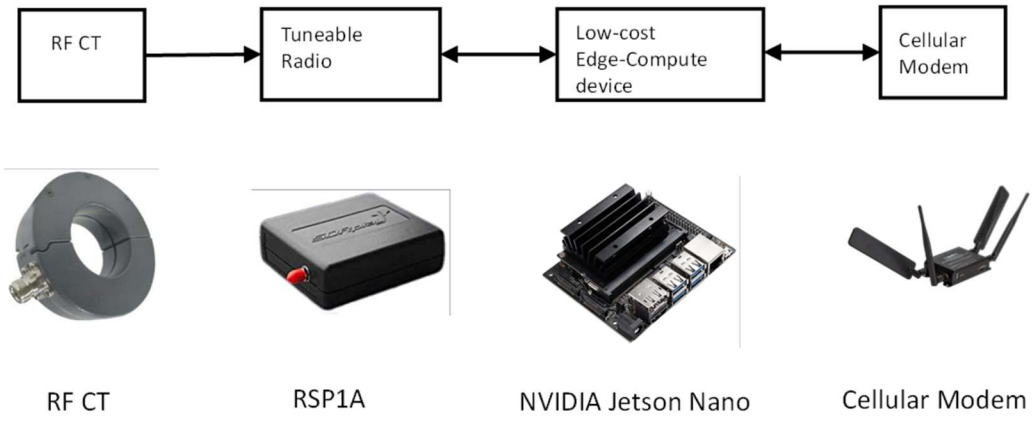

FIGURE 1.4: Proposed system. Top: Block Diagram. Bottom: Photographs of system components.

This goal of this thesis was to develop hardware that could enable the rich pattern-recognition needed to unlock the value of EMSA. Subject Matter Experts note that the greatest value comes from the patterns observed at each frequency. Therefore, the need is to develop a solution with the robustness to sweep entire frequency spectrum, be able to store and analyze the runtime data without losing any patterns, faster in collecting data with lost cost and capability to leverage the power of machine learning. A Software Defined Radio (SDR), which is a radio communication system that uses software for modulation

and demodulation of radio signals, coupled with an edge-computing device such as the NVIDIA Jetson Nano which is capable of highspeed computations as well as deploying machine learning models for anomaly and fault detection, and a Radio Spectrum Processor – RSP1A, which can turn a computer into a general purpose spectrum analyzer, are the proposed hardware solution in this thesis.

Using a device such as the NVIDIA Jetson nano would enable remote monitoring as well as connection with the cloud despite it being an edge-computing device. Real-time monitoring, with low cost, high fidelity, and ease of deployments at remote locations due to the overall size of the proposed solutions, are some of the benefits over the previous approach to EMSA.

1.3 Summary

The remaining chapters of this thesis describe the technology that has been developed and tested. Chapter 2 first provides a comprehensive literature review. It describes common problems in large motors and generators, and it then describes the shortcomings of the existing EMSA approach. Chapter 3 details the solution that has been developed based on feedback from utility stakeholders. Chapter 4 describes results from field tests conducted at a nearby combined-cycle power plant. Chapter 5 provides conclusions and next steps in the technology-development process.

CHAPTER 2: LITERATURE REVIEW

Because failures in electric machines can be so impactful, significant effort has been used to develop fault-detection technologies. This chapter reviews some important background on these topics. Section 2.1 first describes common faults. Section 2.2 then reviews some common fault-detection techniques. Section 2.3 describes a technique known as partial-discharge analysis (PDA). This approach is used to detect early-stage failures in machinery windings. Section 2.4 finally reviews the existing approach to Electromagnetic Signature Analysis.

2.1 Review of Common Machinery Faults

Several studies have documented the major sources of failure in large induction motors [1], [2], [3], [4]. The findings from each are somewhat similar. TABLE 2.1, for instance, summarizes the findings from [3] and [4]. These results list the component that ultimately caused a complete failure. Typically, these faults begin as various mechanical, thermal, and electrical stresses slowly degrade individual components. In the case of stator-related failures, for instance, the majority are caused by degraded insulation. These failures often start as small breaks in winding insulation, perhaps caused by vibrations. Over time, they develop into catastrophic failures such as phase-to-ground short circuits. Similarly, most rotor-related faults are caused by faulty squirrel cages, in which individual broken rotor bars lead to completely cracked cages. The most frequently failed components are bearings, which account for nearly 40% of all issues. Other studies have shown similar results for large generators [27].

TABLE 2.1: The most common motor failures by percentage.

Failed Component	From [3]	From [4]
Bearing	44	41
Stator	26	36
Rotor	8	9
Other	22	14

Early detection of the underlying causes of the failures discussed here are the goal of any monitoring system. The next section discusses the most common methods.

2.2 Common Motor Health Monitoring Methods

Multiple different methods have been developed to detect motor faults, some of which have been used commercially and others of which have only been explored in laboratory environments. This section provides a very brief introduction to some of the most common techniques.

2.2.1 Vibration Monitoring

Vibration signals are commonly used to detect critical motor faults, such as bearing failures, structural resonances and foundational issues, mechanical imbalances, and winding damage. Vibration measurements are provided by accelerometers and proximity probes. These additional sensors and their data-acquisition systems can be very costly, but they are known to provide a high level of detail about the early-stage development of many catastrophic issues, particularly those related to bearings. Because of their cost, they are typically only used in the most critical applications and for the largest motors in major power plants and industrial facilities. Several manufacturers provide both dedicated

monitoring solutions as well as handheld instruments that can be used for periodic spot checks [32][5].

2.2.2 Thermal Monitoring

Thermal monitoring of electric machines can be performed in various ways, including handheld infrared cameras and onboard installed sensors such as thermocouples or resistance temperature detectors. Thermal measurements can indicate the existence of overheated bearings and windings. Such issues typically arise in the latter stages of a fault and just before a major issue is about to occur. Infrared thermography is commonly used to perform spot checks to detect developing anomalies. Devices such as thermocouples and resistance temperature detectors (RTDs) are embedded into large motors for last-minute protection purposes[33][33].

2.2.3 Electrical Monitoring

Electrical monitoring is one of the most attractive methods for real-time analysis because electrical sensors, namely voltage and current transducers, are very easy to install and are essentially required in most large motor applications. The most powerful electrical technique is motor current signature analysis (MCSA). The sections below describe the traditional approach to MCSA as well as some modified approaches that have been developed over time.

Traditional MCSA

Various tell-tale signals are known to exist within the stator current an electric machine. For instance, various higher order electromagnetic interactions within the motor cause effects such as broken rotor bars to induce small signals within the stator current. These signals are typically monitored using frequency-domain approaches such as spectral estimation [7]. This approach has been successfully shown to detect issues such broken rotor bars, eccentric rotors, and faulty bearings. [7],[8],[9]. The next section provides more details on this approach, which has been successfully commercialized [9].

Extended Park's Vector Approach (EPVA)

Several MCSA-variant methods exist. These methods typically include some additional pre- or post-processing approach on the measured current. In the case of EPVA, the terminal voltages and currents are transformed into a rotating reference frame in which the currents and voltages are represented in a complex plane with a direct axis and quadrature axis [8]. The so-called Park's vector will rotate around this plane and trace out a circle when the machine is healthy. If the pattern becomes elliptical, a fault is believed to exist [8]. This approach is found in commercial systems [9].

Instantaneous Power Signature Analysis (IPSA)

This, too, is a variant of traditional MCSA in which the measured voltages and currents are used to develop an instantaneous power signal. This waveform can be examined in the frequency domain and can potentially provide more information about faults than those methods based solely on the current [8].

Motor Voltage Signature Analysis (MVSA)

Stator voltage has also proven to be useful in motor health monitoring, largely because unbalanced or distorted voltages can cause numerous other motor faults such as overheating and uneven rotation (i.e. eccentricity). Several commercially available MCSA systems also monitor voltage as a part of their standard offering [9].

2.3 Partial Discharge Analysis

Some 30 to 40% of all motor failures are caused by faulty stator windings [1], [2], [3], [4]. These issues typically manifest as phase-to-ground or phase-to-phase short circuits, but they begin initially when winding insulation slowly starts to degrade. Early-stage deterioration often causes turn-to-turn faults, in which two or more turns of a single coil are short-circuited. The current in the shorted turns is substantially higher than the operating current and thus this additional current increases the winding temperature to the point at which more severe damage can occur. This is the primary reason why turn-to-turn faults are the original precursor to more severe issues [6]. Although thermal monitoring can indicate such critical issues, the temperature typically does not increase significantly until catastrophic failure is imminent.

An alternative approach to detect early-stage issues is to use probes that can detect the existence of so-called partial discharges that occur when dielectric breakdown happens between windings. The existence of this discharges is an early indicator of stator insulation failure. These methods have been found useful at voltages above 4kV, and various commercial systems are available [7]. For low voltage motors, no comparable method exists [7].

Figure 2.1 provides a basic working explanation of partial-discharge analysis. The image on the left side of the figure shows a high-voltage cable with a grounded outer conductor. The image on the right shows a circuit model for the cable. During normal conditions, there is a capacitance between the cable and the outer conductor. C4 represents this bulk-capacitance. If a defect forms inside the insulator, there will be a pathway through the insulator that includes the defect. This pathway is represented by the series connection of C1, C2, and C3. If the voltage difference between the two conductors becomes high enough, dielectric breakdown can occur inside the defect [16], [18].

Figure 2.2 shows how dielectric breakdowns occur inside of a defect. As the AC voltage on the conductor rises throughout a cycle, the voltage across the defect also increases. Once the voltage is high enough to cause dielectric breakdown, an impulsive current flows between the high-voltage inner conductor and the grounded outer conductor. This current, which has a waveshape like that of the red curve shown in Figure 2.2, lasts only several microseconds and can be measured with appropriate equipment such as radio-frequency current transformers (RFCTs) [16], [18].

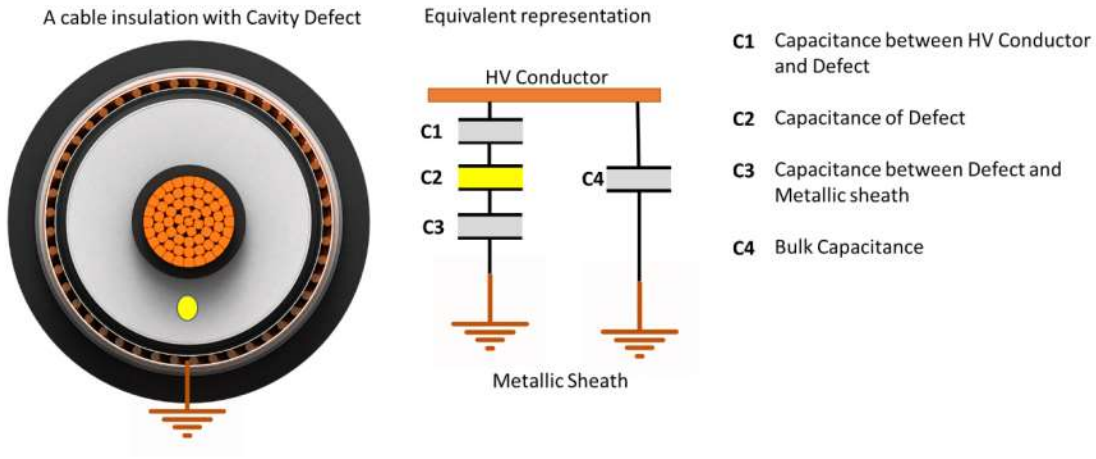

FIGURE 2.1: Basic working explanation of partial discharge analysis[30].

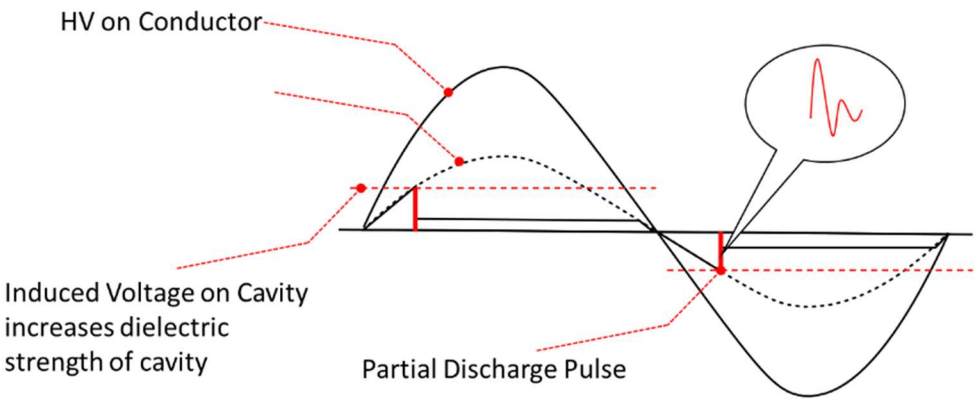

FIGURE 2.2: Dielectric breakdown inside a defect[30].

The process described in Figures 2.1 and 2.2 occurs inside large electric machines when insulation begins to fail between windings[30]. Partial discharge analysis can be used to detect partial discharges, but it is difficult to apply in practice. To use it, one must measure the current flowing through a capacitor connected between ground and one of the stator windings. Many utilities are worried the measurement capacitor will fail, and so the technique is only used during outage periods when the machine is offline [16], [18].

2.4 Electromagnetic Signature Analysis

Chapter 1 introduced the basic concept behind electromagnetic signature analysis (EMSA). This technique has been used in the power industry to detect early-stage faults in large motors and generators. EMSA has been most successful in detecting stator-winding issues such as partial discharges, internal arcing, corona discharges, and gap discharges. These are all short-term, impulsive electrical events, and thus they generate wide-band signals. Partial discharges, for instance, can be so quick that they generate signals with bandwidths upwards of 1000MHz. At such frequencies, machines can act as

antennae, thus transmitting electromagnetic waves indicating the existence of early-stage faults. EMSA is the use of such signals for fault detection. These signals are often referred to as electromagnetic interference (EMI). Under guidance from EPRI, the power industry applies EMSA between 30kHz and 100MHz. Figure 2.3 shows the frequency ranges associated with various faults. Note that partial discharges, for example, are believed to occur above about 20MHz [14]. EMSA is a promising technique, but it is expensive to implement in a continuous, online manner. Additionally, it is only useful on machines with voltages high enough to generate partial discharges and other phenomena (i.e. >4kV) [14].

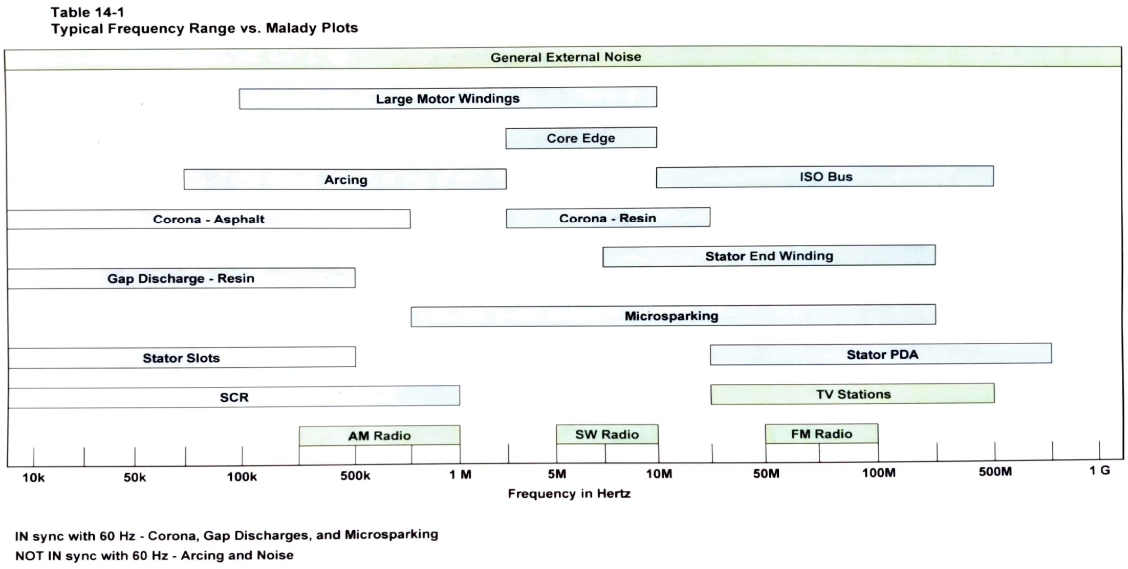

FIGURE 2.3: Failures corelating to certain frequency ranges[14].

Chapter 1 noted that EMSA can be performed using simple hand-held radios called "sniffers" located next to the equipment. The technique works well since faults generate waveforms measurable by radio receivers. Unfortunately, it does not lend itself to continuous operation [14]. Large utilities have adopted a standard approach that uses permanently installed equipment. Figure 2.4 shows a typical setup. This figure shows a

spectrum analyzer and other related equipment. The spectrum analyzer receives a signal from a sensitive, split-core, broadband radio frequency current transducer (RFCT). This device is attached to the frame ground lead or power conduit of the machinery under observation, as shown in figure 2.6 This RFCT is connected to the spectrum analyzer via a double shielded coaxial cable [14].

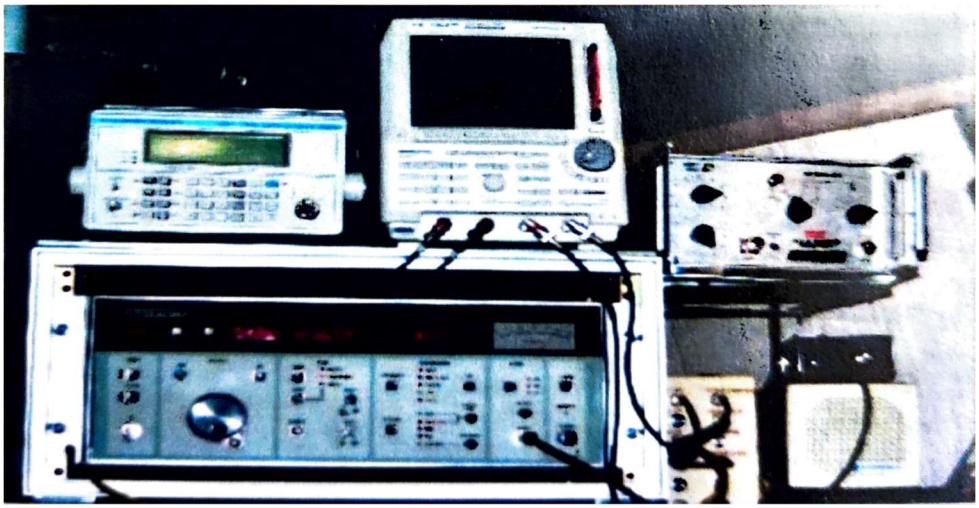

FIGURE 2.4: Typical EMSA equipment[14].

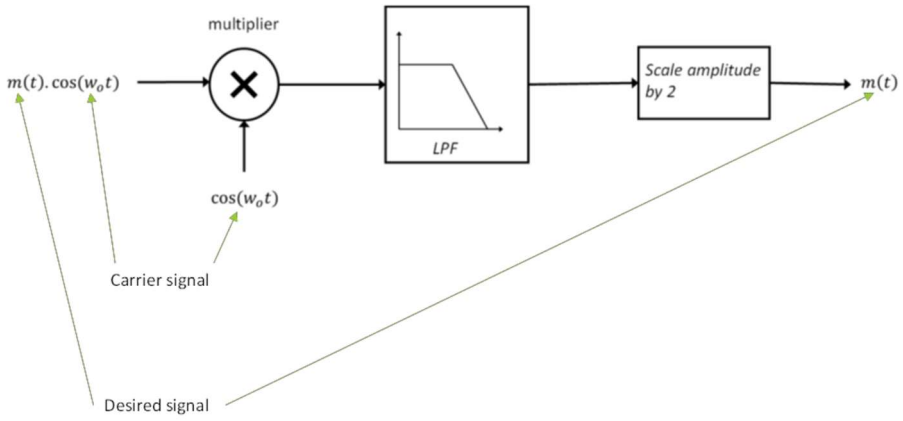

FIGURE 2.5: EMSA approach: Amplitude demodulation at a given frequency[14].

Figure 2.5 shows the measurement technique used in EMSA. The signal from the RFCT is fed into the spectrum analyzer, which is tuned to a particular frequency, starting from 30kHz. The process shown in Figure 2.5 is amplitude demodulation. The received signal, which is denoted as $m(t)\cos(\omega_0 t)$ is multiplied by another signal and then passed through a narrowband low-pass filter and some further amplitude scaling. The output of Figure 2.5 is the component of $m(t)$ that falls within the bandwidth of the low-pass filter[29]. This process is implemented inside the spectrum analyzer.

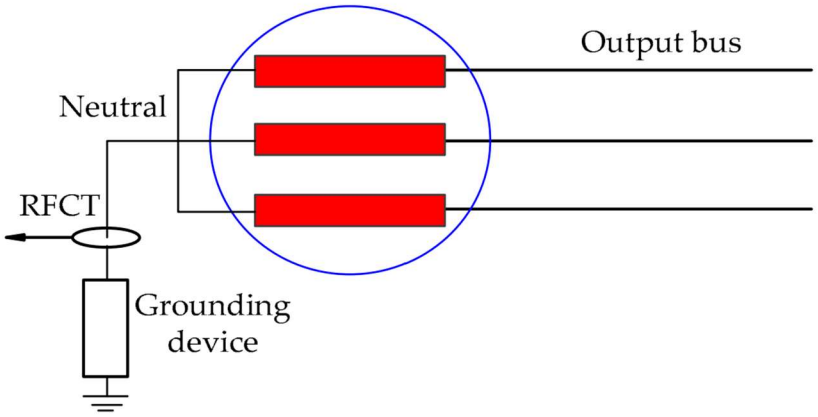

FIGURE 2.6: Schematic of RFCT connected to the neutral ground lead[15].

Figures 2.7 and 2.8 show how the process is implemented across the frequency spectrum. The frequency of the signal feeding into bottom of the multiplier shown in Figure 2.4 is first set to 30kHz. As shown in Figure 2.8, the output is recorded for 90ms. This demodulated signal is passed through a quasi-peak (QP) detector or averaging (AV) circuit. This provides a single statistic quantifying the amount of content at a given frequency. This value is placed in a frequency spectrum plot as shown in Figure 2.8. The process shown in Figure 2.7 is repeated for 8000 difference frequencies between 30kHz and 100MHz [14].

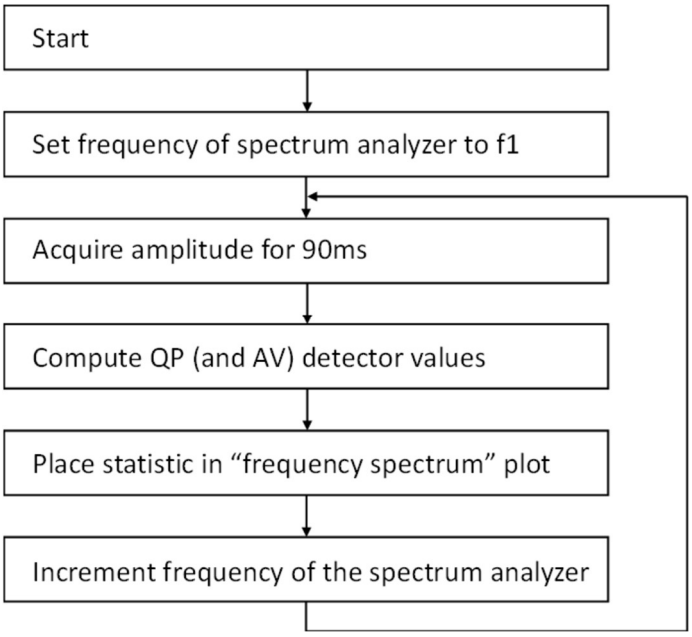

FIGURE 2.7: Flow chart of current EMSA approach.

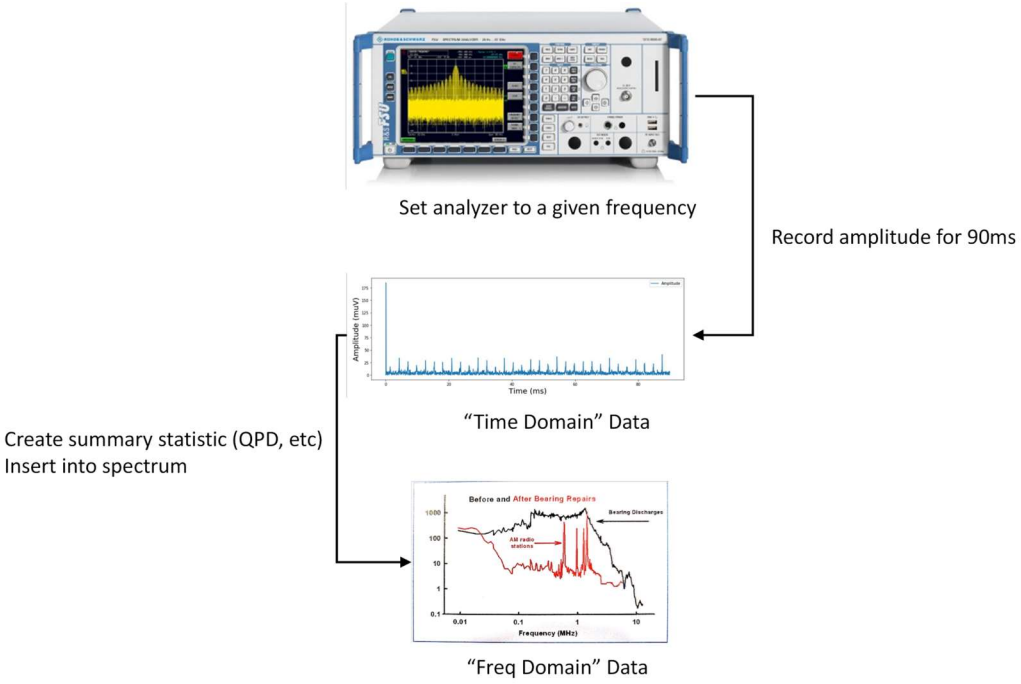

FIGURE 2.8: Block diagram summarizing the EMSA approach, recording data for given frequency[14].

2.5 Shortcomings In the Existing Approach To EMSA

Chapter 1 noted that this thesis proposes a new approach to EMSA. This work started when utility partners noted several shortcomings with the existing approach. Most importantly, these partners described major failures that were not detected (P. Lesner, personal communication, August, 2021) by the method described in Section 2.4. This section provides the technical reasons for these missed detections, as well as some practical problems associated with existing EMSA technology.

2.5.1 Nature Of Recorded Data

Chapter 1 noted that EMSA started when maintenance staff first noticed that certain failures created signals that could be "heard" on handheld radios. Staff made statements such as corona discharge sounds like "frying bacon" and gap discharges sound like "popping." [14]. Human-based pattern recognition was thus applied to time-domain signals. Figure 2.9 shows the patterns associated with several faults.

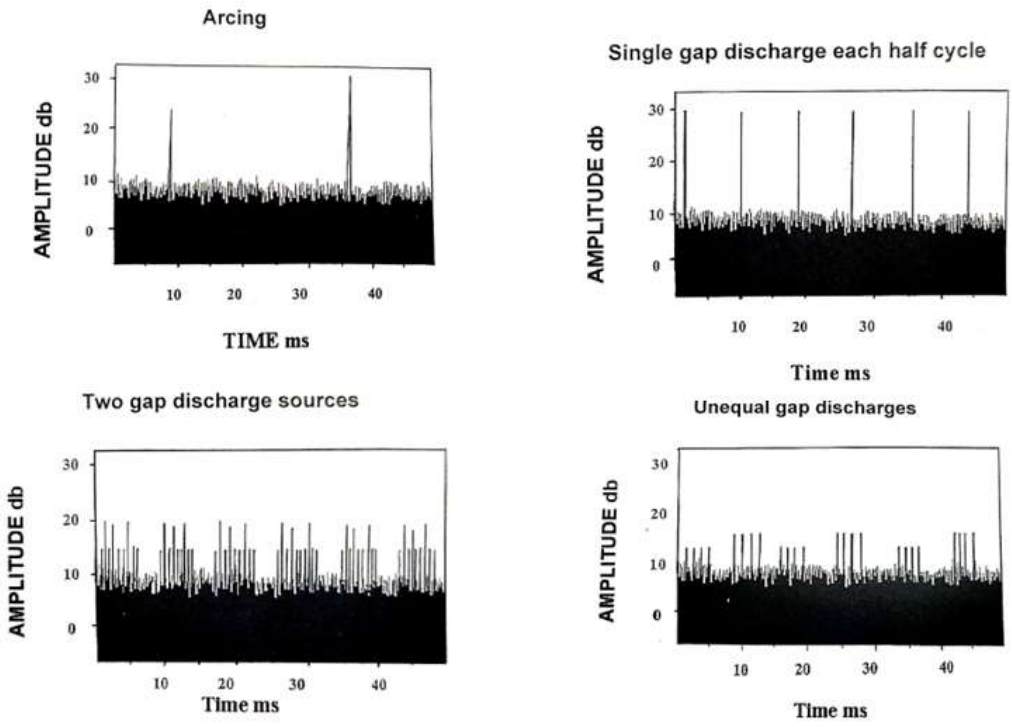

FIGURE 2.9: Patterns corelating to different fault phenomenon[14].

The time domain data recorded in Figure 2.9 is very large. For 90ms, there are about 28,800 data points per frequency. With 8,000 frequencies, it is almost impossible to store this amount of data in real time. To circumvent this problem, utilities started to compute the QP value as a summary statistic, thus leading to only 8,000 values per frequency sweep. This leads to the loss of the essential patterns which could be very essential in fault detection.

Figure 2.10 shows how a quasi-peak detector works. It is very similar to an AM radio detector circuit. The top image shows typical pulses that might be observed at the output of process shown in Figure 2.5. The capacitor charges when large pulses appear, and it discharges when the incoming signal is too small to forward bias the diode shown in the schematic. The average value at the output of the QP detector circuit is taken as the output[29].

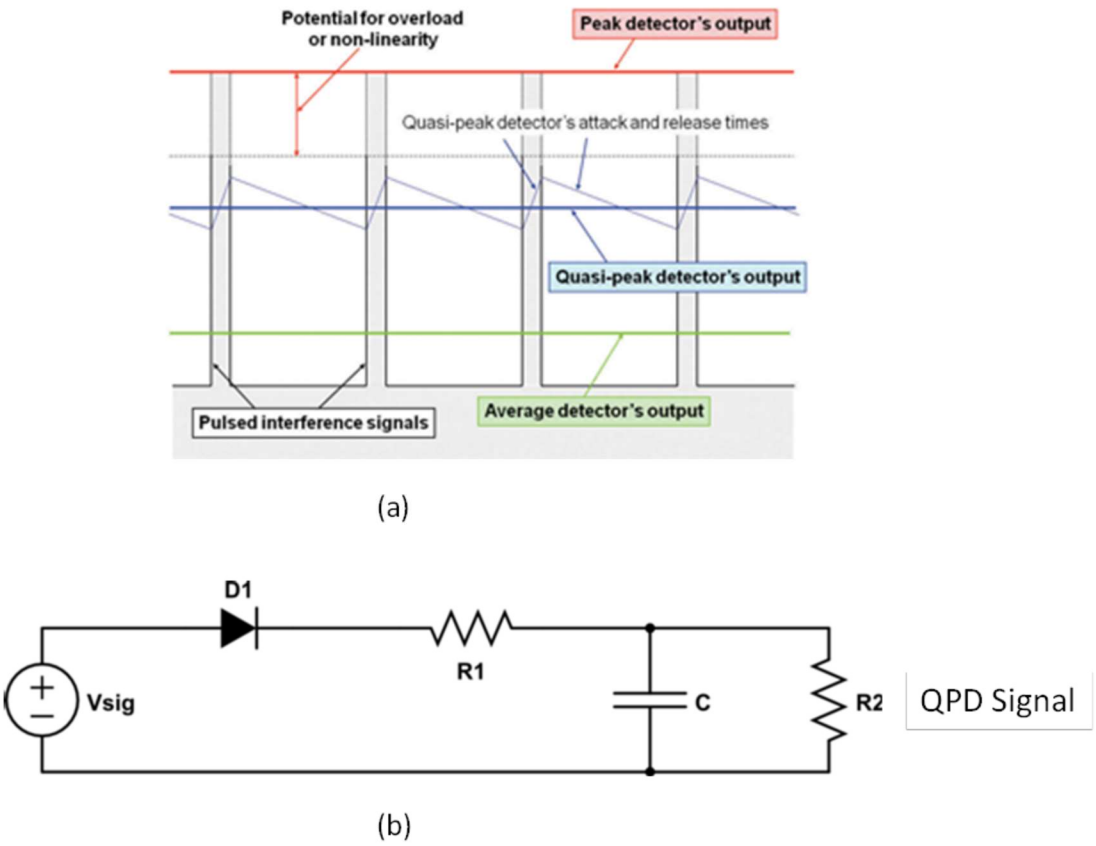

FIGURE 2.10: (a) The charging and discharging of a quasi-peak detector. (b) a simple circuit showing a simple quasi-peak detector circuit.

Using the QP detector causes the valuable time-domain patterns to be lost, but this is not the only problem. Figure 2.11 shows two signals that produce the same QP value. Clearly, both signals are very different, and the one on the left indicates a fault. This would not be perceptible, however, using only the QP value.

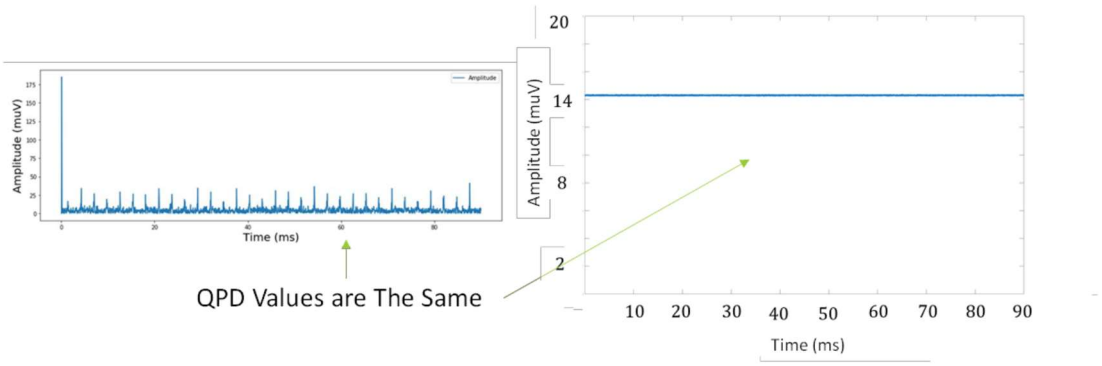

FIGURE 2.11: Time-domain patterns lost when data is compressed into a single summary statistic.

2.5.2 Time Required for A Single Sweep

Section 2.4 described how utilities sweep through 8,000 frequencies, recording 90ms of data at each one. This process thus requires at least 12 minutes. This is a very large amount of time taken considering most of the data is thrown away after extracting just a single number from the quasi-peak detector output for each frequency. There is also a concern that data recorded at the end of the sweep could be uncorrelated with data recorded at the beginning.

2.5.3 Radio Station Interference

As noted, EMSA started by observing radio signals near large machinery. Many faults have been found to create signals in the AM and FM radio bands. Unfortunately, the RFCT detects radio signals as well. Utilities have noted difficulty in being able to distinguish faults from radio signals. Figures 2.12 and 2.13 show how AM and FM radio stations present at frequency ranges where faults can be present and might go unnoticed due to radio station interference.

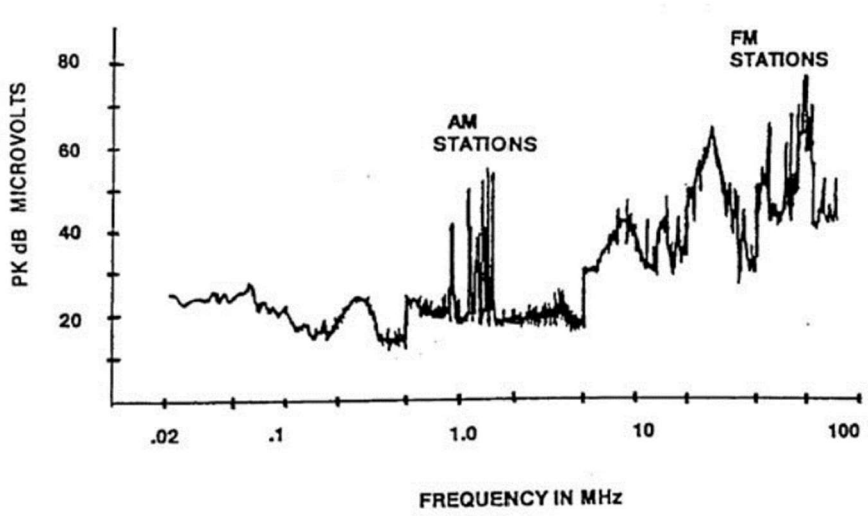

FIGURE 2.12: AM and FM radio stations present dominantly causing faults not being detected by RFCT.

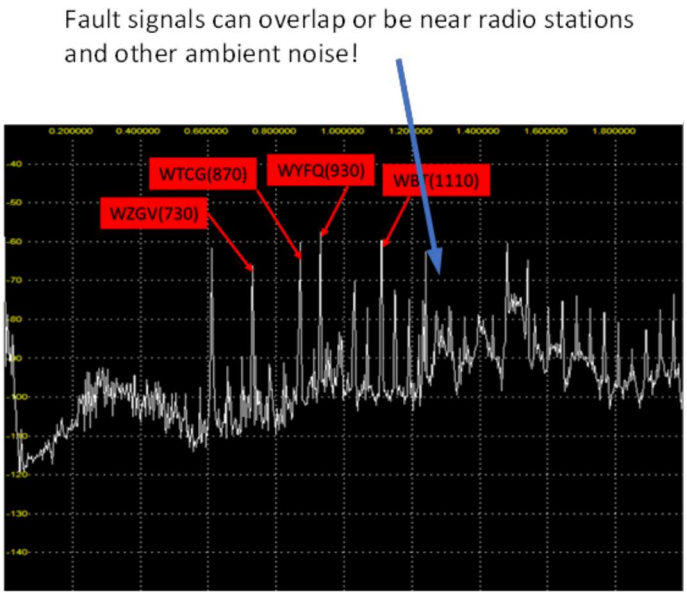

FIGURE 2.13: Overlap between ambient radio signals and fault signals.

2.5.4 High Cost of Equipment

The current EMSA approach uses a spectrum analyzer with custom software. This spectrum analyzer is costly. It is difficult to scale this solution across many locations. Chapter 1 described the growing reliance on distributed generation. The current hardware solution could not be scaled across a large renewable fleet.

CHAPTER 3: METHODOLOGY

This Chapter reviews the methodology proposed in this thesis to implement EMSA. Section 3.1 discusses the overall idea and reason why choosing the proposed approach over the current approach, 3.2 discusses the operation of Software Defined Radio (SDR), which is the core technology. Section 3.3 reviews the complete approach that has been developed using the SDR. Section 3.4 discusses some practical challenges that needed to be overcome to deploy the technology in the field.

3.1 Overall Concept

Section 2.4 described how EMSA is performed by measuring the average amplitude at 8000 different frequencies detected by the RFCT. This process takes significant time, disregards critical time-domain patterns, and requires expensive hardware. The alternative approach proposed in this thesis was developed by carefully examining field data. Figure 3.1 shows the output of the RFCT in a nearby power plant below 7MHz. This signal contains many pulses of varying amplitude and a small noise floor containing narrowband signals such as AM radio signals. The nature of this signal is not surprising given the findings of the literature review in Chapter 2. Stator faults cause short-duration, wideband pulses. The signal in Figure 3.1, for example, includes a pulse train repeating at approximately 360Hz. Wideband signals of this variety have content at many frequencies. The EMSA approach described in Chapter 2 is a narrowband technique used for AM radio. A signal such as the pulse train shown in Figure 3.1 will thus have the same amplitude at many different frequencies. Using a narrowband approach to classify wideband signals

produces significantly more data than needed. Narrowband measurements are a natural choice given that EMSA started when operators walked around listening for faults on handheld radios. With a clearer understanding of fault behaviors and a focus on modern computing tools, more appropriate techniques can be developed.

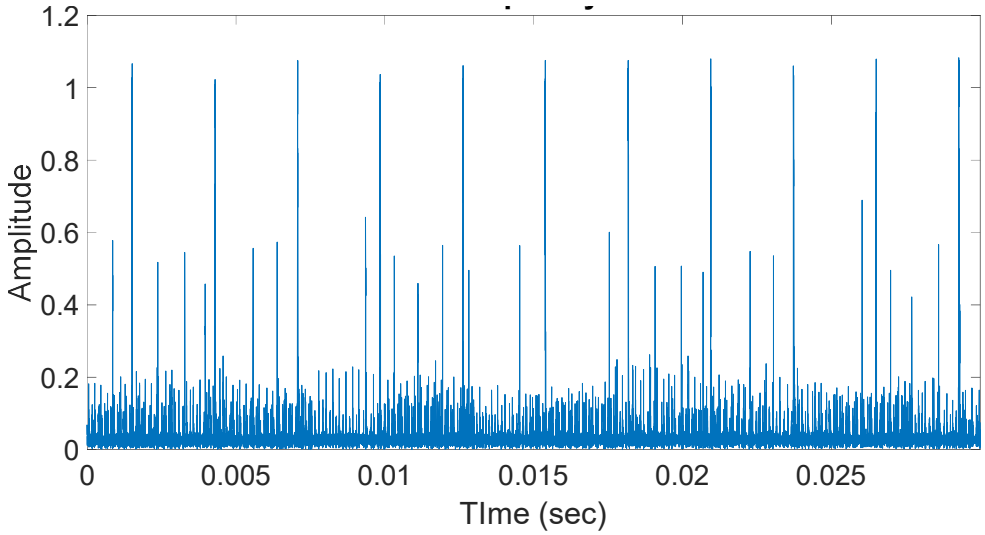

FIGURE 3.1: Measured RFCT signal below 7MHz.

This thesis proposes an alternative approach focused on capturing wideband signals. Instead of using a narrowband low-pass filter as shown in Figure 2.4, one could use a wideband filter and increase the frequency in much coarser steps. Depending on the quality of the hardware, this leads to significantly fewer data files and a much quicker sweep time.

This thesis also investigates the use of modern low-cost hardware. Instead of using a costly spectrum analyzer, we use a software-defined radio that can make similar measurements with lower accuracy. It is not clear if this accuracy is needed since there is a limited understanding of how large the fault signals should be. This issue requires further investigation, but the initial results described below are promising.

The proposed system also includes a low-cost edge-compute platform that can acquire and store the recorded data files. It can extract features from the time-domain data and implement machine-learning algorithms without having to send the data files over the network.

3.2 Proposed system

Figure 3.2 shows the block diagram of the proposed system. The primary goal of this system is to implement the improvements described in Section 3.1. The following sections describe each component.

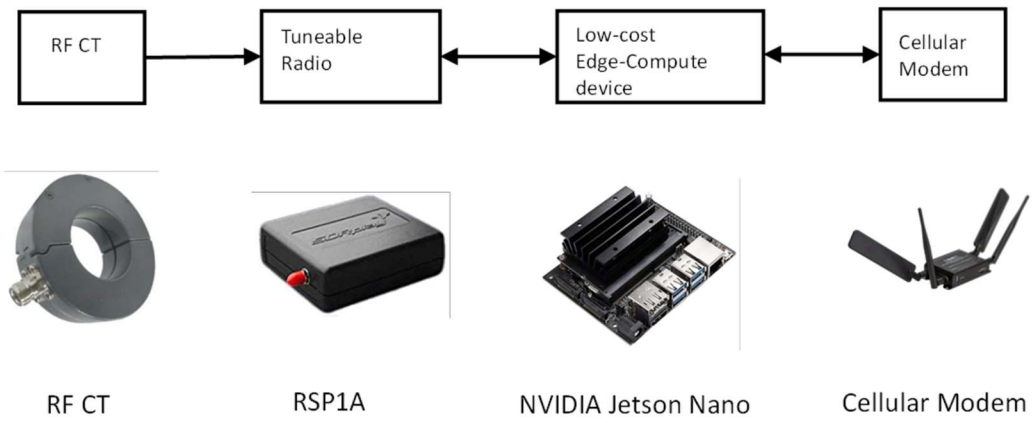

FIGURE 3.2: Elements of the proposed system.

3.2.1 Radio-Frequency Current Transducer

The first element shown in Figure 3.2 is the radio-frequency current transducer (RFCT). Section 2.1 described how high-frequency signals are generated by faults such as partial discharges that occur inside of electric machines. As described, these signals generate common-mode currents that flow through the ground of machine. Figure 2.5

shows that the RFCT is connected to the neutral ground for measurements in on-line partial discharge. Figure 3.3 shows how the RFCT is connected to the ground line of steam-turbine engine for measure the signals in this thesis. RFCTs are commonly used in EMSA [14].

FIGURE 3.3: RF-CT (marked in red) connected to the neutral ground.

The selected RFCT is the F-69 from Fischer Communications[25]. This device can measure signals from 1kHz to 500MHz, and it has an inner diameter of 70mm. Figure 3.3 shows how this device was installed at the field site as described in Chapter 4. The diameter was selected so that it would fit over the ground line shown in Figure 3.3.

3.2.2 Software Defined Radio

The key technology in this system is the Software-Defined Radio (SDR) shown in Figure 3.1. This device takes the input from the RFCT and converts it to a set of samples that can be easily processed using a low-cost edge-compute platform. SDR can significantly reduce the cost of the installed system. Chapter 2 described how the current approach to EMSA uses a spectrum analyzer, which uses expensive hardware to process radio-frequency signals. The approach proposed here uses the SDR to acquire RF signals, and to convert them into software where most of the signal-processing is performed [13].

Figure 3.3 is a block diagram showing how the SDR works. The output of the RFCT is the input signal $x(t)$. This signal is assumed to indicate a fault and has the form

$$x(t) = m(t)\cos(2\pi f t). \quad (1)$$

The signal is amplitude-modulated and has a carrier frequency f. The input signal passes to a low-noise amplifier (LNA) and then to a series of demodulators that take the signal down to baseband for later processing. As shown in Figure 3.3, the system has a quadrature demodulator consisting of two mixers and an oscillator. The output of the upper mixer is

$$x(t)\cos(2\pi f_c t) = \frac{1}{2}m(t)\cos(2\pi(f_c - f)t) + \frac{1}{2}\cos(2\pi(f + f_c)t)$$

and the output of the lower mixer is

$$x(t)\sin(2\pi f_c t) = \frac{1}{2}m(t)\sin(2\pi(f_c - f)t) + \frac{1}{2}\sin(2\pi(f + f_c)t))$$

An input signal with $f = 1$MHz will thus produce output signals at both $f_c + 1$MHz and $f_c - 1$MHz. The low-pass filters (LPFs) remove any high-frequency content. The filter

output is sampled by an analog-to-digital converter (ADC) for further processing in a computer.

Figure 3.4 is best understood with an example. Consider a radio with an ADC capable of sampling at 10MHz. The low-pass filters in Figure 3.4 would thus require a bandwidth less than 5MHz to prevent aliasing[29]. If $x(t)$ has a frequency of 63MHz and the radio is tuned to $f_c = 60$ MHz, the two mixers will have signals at 3MHz and 123MHz. Only the 3MHz component will thus pass through the filter to be sampled by the ADC. This approach allows one to use low-cost hardware to sample high-frequency signals by shifting their frequency to baseband (i.e. around DC).

Figure 3.4 shows that SDRs have quadrature demodulators. This means they produce two outputs. These two components are the "in-phase" or "I" component and the "quadrature" or "Q" component. These two signals are captured in the computer in complex form, i.e. [13]

$$y(t) = i(t) + j\,q(t) \tag{2}$$

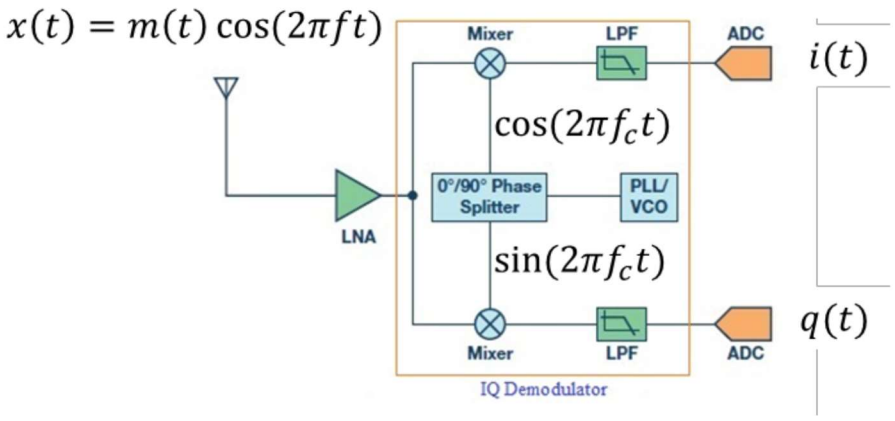

FIGURE 3.4: Working of Software-Defined Radio using I/Q Demodulator[29].

FIGURE 3.5: SDR used – SDRPlay RSP1A[31].

The SDRPlay RSP1A, shown in figure 3.5, is a wideband 14-bit SDR which covers the RF spectrum from 1kHz to 2GHz. It has a 14-bit native ADC (analog to digital converter) with sampling rate from 2 MSPS to 10.66 MSPS. It has 3 resolutions to select from, viz. 12-bit (6.048 - 8.064 MSPS), 10-bit (8.064 - 9.216 MSPS) and 8-bit (> 9.216 MSPS). The proposed approach makes use of the 10-bit resolution of the ADC by using the sampling rate of 9MHz (9 MSPS)[31].

3.2.3 Edge-Compute Platform: NVIDIA Jetson Nano

The proposed approach leverages the availability of low-cost edge computing. The ouptuts of the SDR are sampled by the edge-compute platform. This device can quickly acquire data, extract features, implement pattern-recongition algorithms, and send the results to the cloud.

The selected platform is the NVIDIA Jetson Nano 4GB [26]. This device hosts a 128-core Maxwell GPU and an ARM Cortex A57 Quad-Core CPU with a maximum operating frequency of 1.43 GHz. Ubuntu 18.04.6 LTS (Bionic Beaver) is the operating system. Figure 3.6 shows the NVIDIA Jetson device used. The RSP1A is connected to the Jetson Nano via a USB cable. Figure 3.2 indicates that the Jetson Nano is also connected to a cellular modem so that data can be acquired remotely.

FIGURE 3.6: NVIDIA Jetson Nano 4GB developer kit[26].

3.3 Software Development for Data Acquisition

Software was developed to use the system described in Section 3.2. This section describes each individual component.

3.3.1 Overview

Figure 3.7 shows the flowchart of the developed software. The radio is tuned to an initial center frequency of 3MHz. Raw time series data of the form $i(t) + jq(t)$ is collected for one second, and this data is saved in a binary file. The frequency is incremented in steps of 3MHz, with a two-second delay after each frequency change. The RSP1A sweeps the entire frequency spectrum from 3MHz to 100MHz, meaning that 33 frequencies are scanned. After a single sweep, each data file is trimmed to only 100ms.

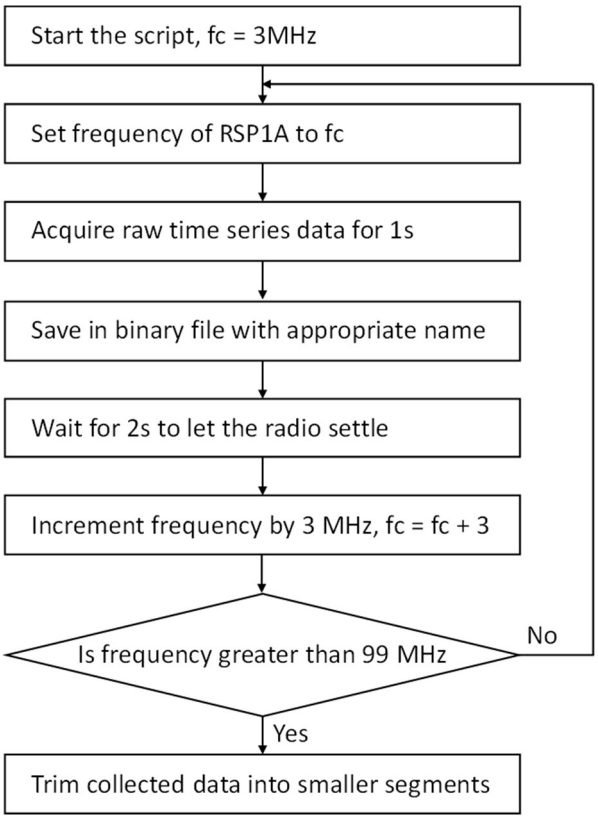

FIGURE 3.7: Flowchart of the proposed system, showing the execution of code for collecting data.

Figure 3.7 shows the graphical representation of the data-collection process. The radio is setup so that the bandwidth of the low-pass filter is $\pm$3MHz. When the radio is tuned to $f_c = 3$MHz, the system acquires data between 0 and 6MHz. When $f_c = 6$ MHz, the radio acquires data between 3MHz and 9MHz. This.process continues as shown in Figure 3.8 until $f_c = 99$MHz.

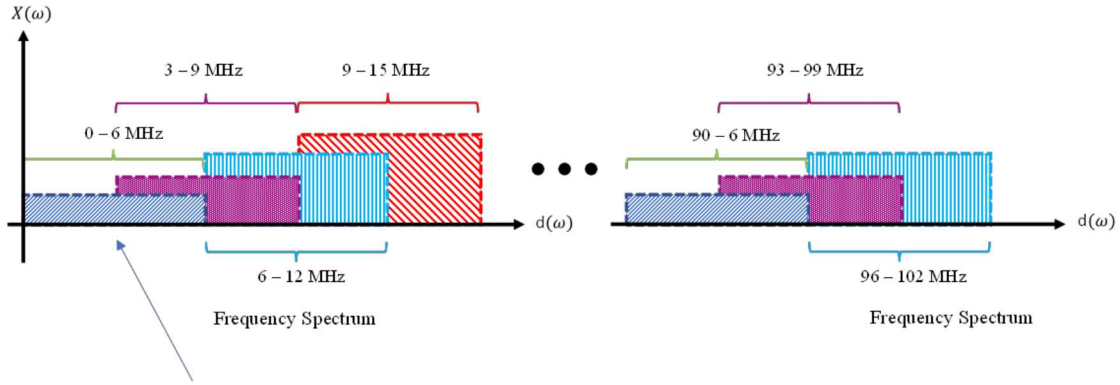

- Window 1: Set $f_c = 3\text{MHz}$ with $BW = 6\text{MHz}$; record raw $i(t) + jq(t)$ for 100ms
- Window 2: Set $f_c = 6\text{MHz}$ with $BW = 6\text{MHz}$; record raw $i(t) + jq(t)$ for 100ms
- ...
- Repeat to $f_c = 99\text{MHz}$

FIGURE 3.8: Graphical representation of data collection at each center frequency, spaced 3 MHz apart from the neighboring center frequency, with a bandwidth of 6 MHz.

The tasks described in Figure 3.7 are performed in a Linux shell script executed on the Jetson NANO. The shell script is called by CRON, a Linux-based scheduling tool that automatically runs twice per hour. The total time for one sweep is 99s.

3.3.2 Programming the Radio

GNU Radio Companion is a graphical software package that allows users to easily program most common SDRs. Users create flowgraphs that show how data should be handled by the radio. The resulting flowgraph is used to create Python code that can be exported for real-time execution on the Jetson NANO.

Figure 3.9 is a snapshot of the flowgraph created in GNU Radio Companion[28]. As the flowgraph shows, data from the RSP1A is saved as a binary file after being converted from a stream of data to a vector. The Automatic Gain Control (AGC) is switched off for

the RSP1A, and the device is tuned to a particular frequency with sampling frequency set to 9MHz. The total number of data points to be collected is set by setting the value for number of items in the “Head” block which copies the first N items to the output then signals done, and this number is set to be the similar as the sampling frequency i.e., 9 mega samples. This results in the data being collected for 1 second per frequency band.

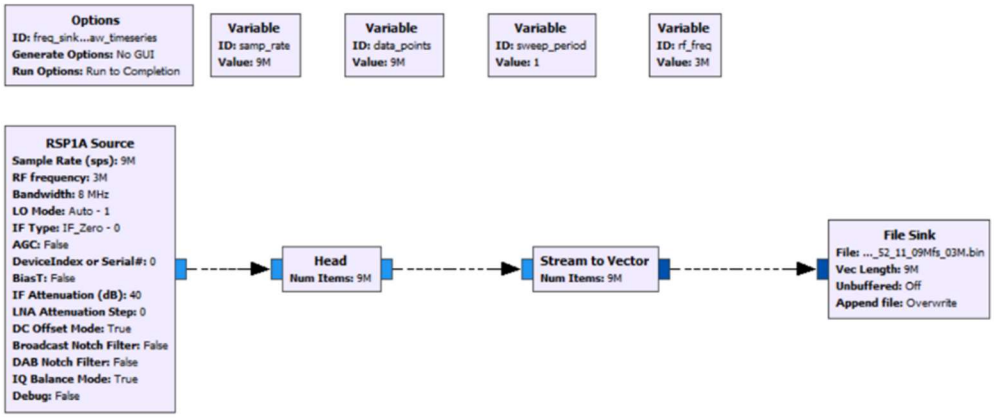

FIGURE 3.9: Flowgraph used in GNU Radio Companion.

Data collected by the RSP1A is raw time series data obtained by tuning the radio to the desired frequency. The “Stream to Vector”, converts the stream of raw time series data received from RSP1A into a vector of the given size. This vector is then saved into a binary file with name created by combining the timestamp, the sampling frequency, and the center frequency of the radio, e.g., 2022_05_21_15_46_03_09Mfs_03M.bin indicates that the file was created on 21st of May 2022 at 15:47:03 with 9MHz as the sampling frequency and the radio tuned at 3MHz.

As explained in section 3.1.2, a baseband signal would have I and Q components. The RSP1A records the data for any given frequency such that the I and Q values for any given datapoint are recorded sequentially. Hence, even after setting the number of items to be recorded to 9MS, it means 9 million such samples each with I and Q data components,

summing up to total of 18 mega samples recorded within 1 second of time. These I/Q components of any data points are stored in a vector, as suggested by the "Stream to Vector" block, and this vector stores I/Q components of each data point sequentially - thus the first data point will have its I/Q components value stored and then the second data point will have its I/Q components value and so on and so forth. So, the vector will look like $[i_1 \quad q_1 \quad i_2 \quad q_2 \quad i_3 \quad q_3 \quad \ldots q_{n-1} \quad i_n \quad q_n \ ]$ where n is the number of items to be recorded as mentioned in the "Head" block.

3.3.3 Challenges During Data Collection

The software (proprietary API of RSP1A radio) used for recording data and writing to a binary file, has a drawback of not being able to correctly record the data in the very first cycle of the signal being recorded when the radio to a particular frequency. For example, when the radio is switch to 3 MHz at the beginning the data collection process, the very first 16.66 ms worth of data is polluted with garbage values overwritten on the collected data, and when the radio is switched to following frequencies, each time for the centre frequency for the first 16.66 ms (one cycle of a 60 Hz line), data collected is contaminated with garbage values. Therefore, the data trimming piece of software keeps this into account and trims the first 30 ms of data, extracts the next 100 ms and then discard the rest of the 1 sec data.

With the help of equation 3 from section 3.1.2, the raw time series data over 30 ms is collected by taking the summation of absolute value of the data points with complex data. Equation 3 is used for plotting the data collected at various frequencies.

$$f(t) = \sum_{(n-1)\Delta t}^{n\Delta t} |i(t) + jq(t)|dt \tag{3}$$

Figures 3.10 to 3.17 show the data collected over 30ms. It can be clearly seen the first 30 ms of data being contaminated, hence being discarded. Even at higher frequencies, the issue persists and was resolved by discarding the first 30 ms of data.

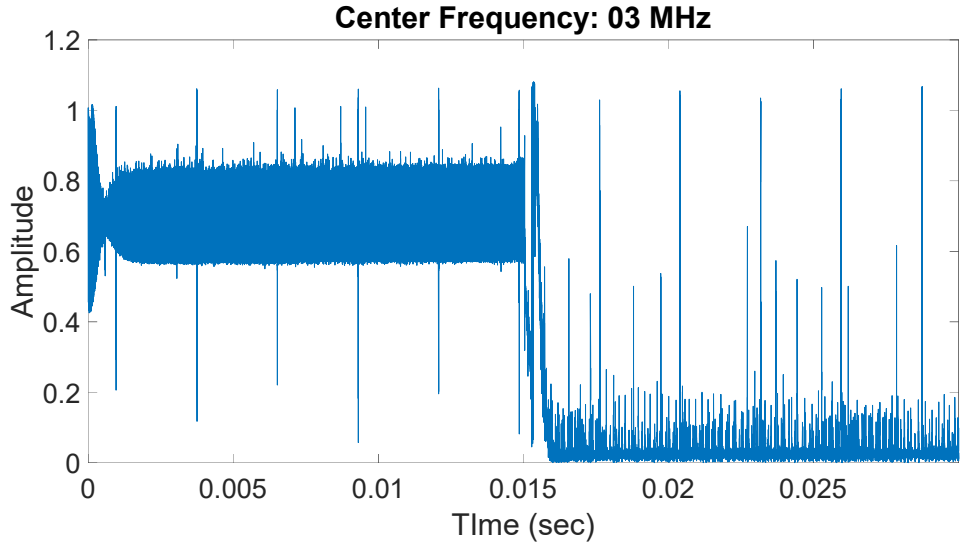

FIGURE 3.10: First 30 ms of data. Radio tuned to 3 MHz.

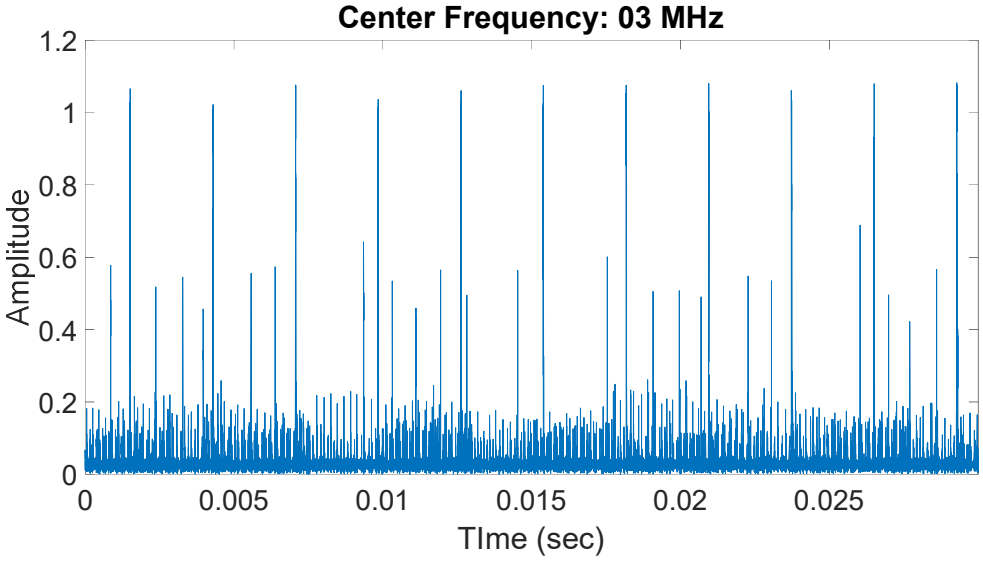

FIGURE 3.11: 30 ms of data from the remaining 1 second of data. Radio tuned to 3 MHz.

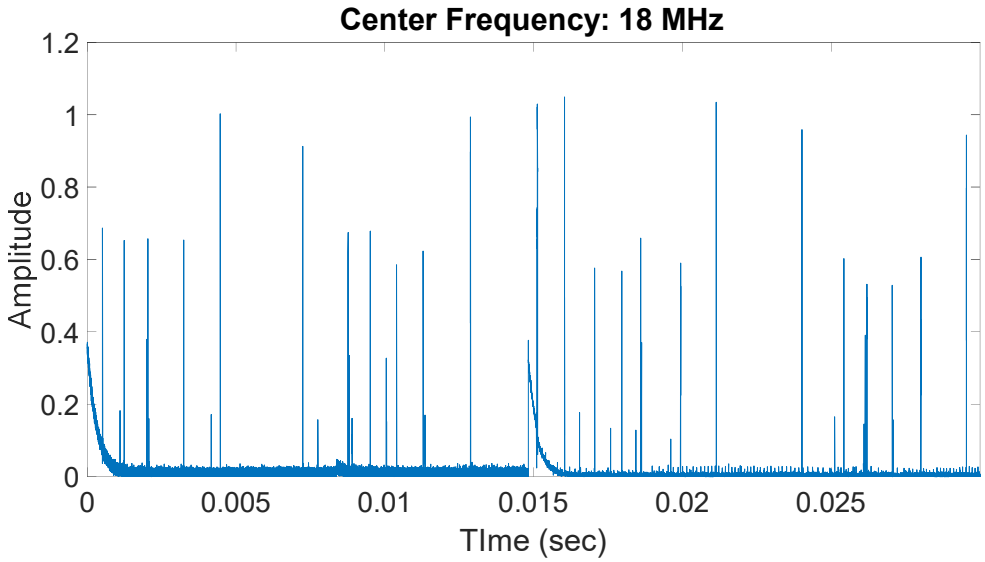

FIGURE 3.12: First 30 ms of data. Radio tuned to 18 MHz.

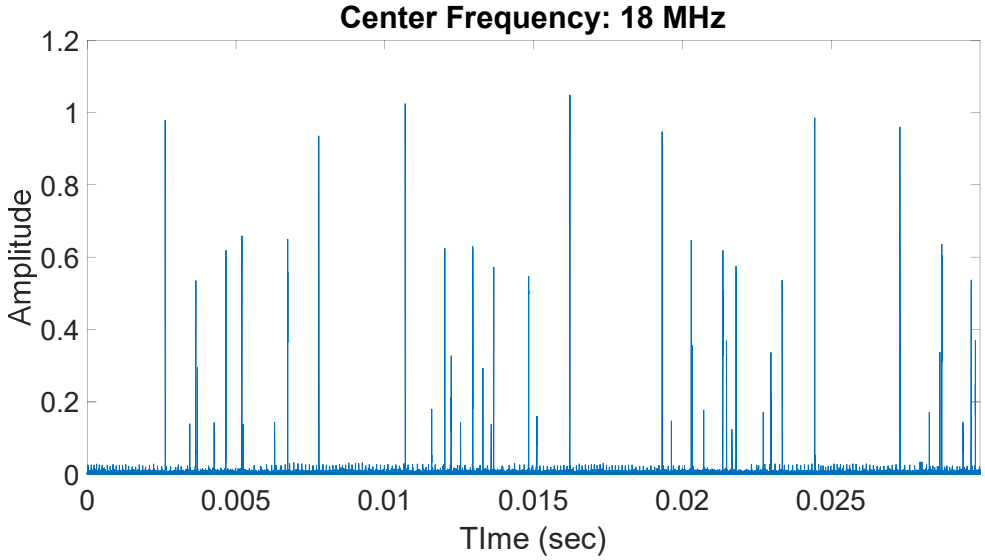

FIGURE 3.13: 30 ms of data from the remaining 1 second of data. Radio tuned to 18 MHz.

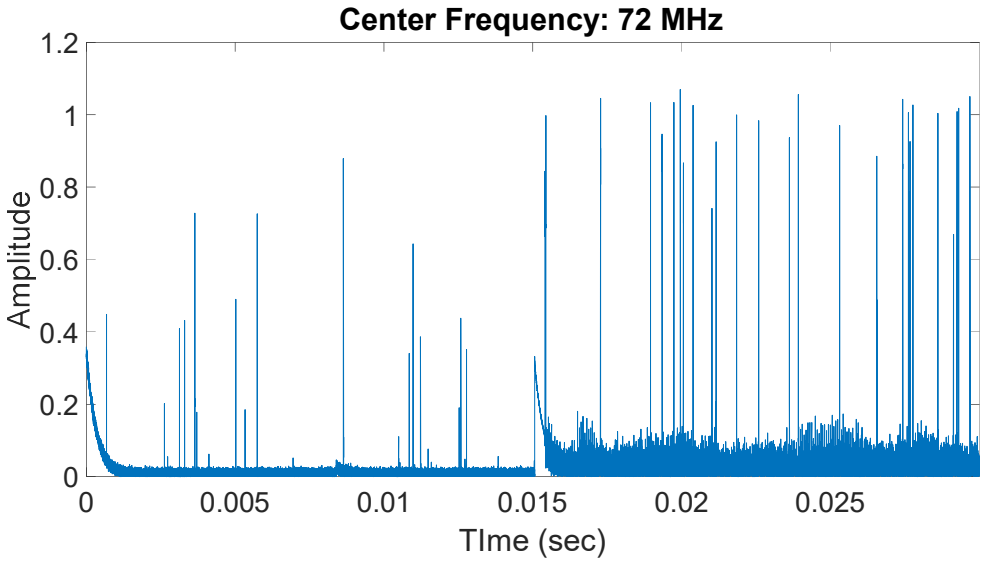

FIGURE 3.14: First 30 ms of data. Radio tuned to 72 MHz.

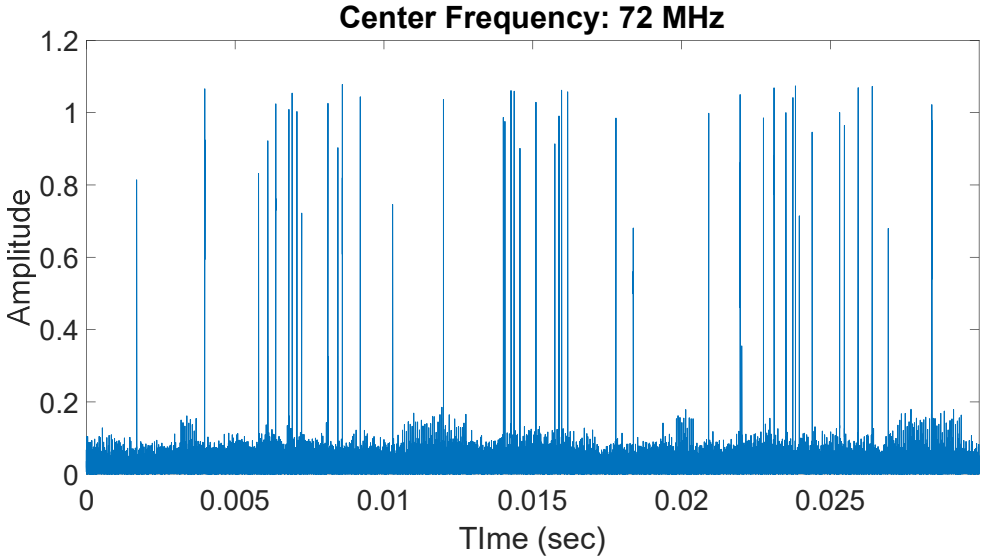

FIGURE 3.15: 30 ms of data from the remaining 1 second of data. Radio tuned to 72 MHz.

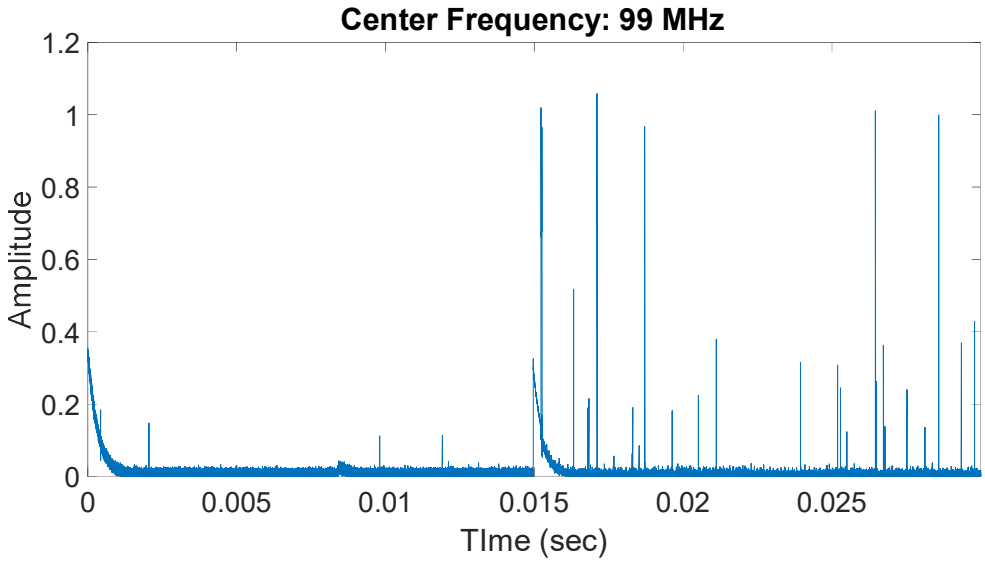

FIGURE 3.16: First 30 ms of data. Radio tuned to 99 MHz.

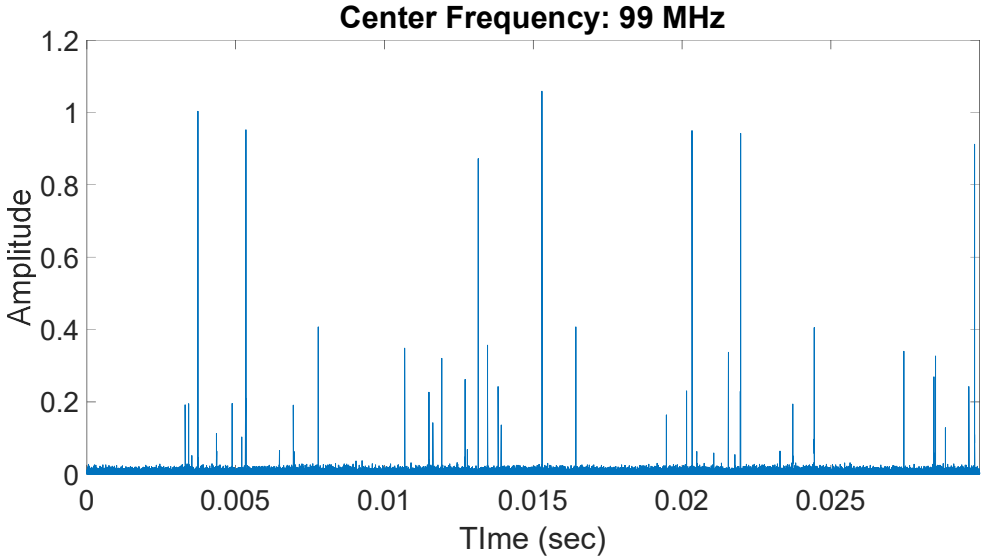

FIGURE 3.17: 30 ms of data from the remaining 1 second of data. Radio tuned to 99 MHz.

CHAPTER 4: FIELD RESULTS

Chapter 4 discusses the results obtained during field testing of the proposed system. Section 4.1 discusses the field setup with the utility partner. Section 4.2 discusses the data collected at various frequencies from 3 MHz to 99 MHz. Section 4.3 discusses two processing techniques used to summarize the data without losing the time-series nature of the collected data.

4.1 Field Setup at Utility Partner Power Plant

The proposed system was installed at multiple locations at a combined cycle plant owned by a utility partner. The system was installed to monitor a 300MW steam turbine and two 180MW gas turbines. Monitoring was performed only briefly on the two gas turbines. The system was installed for several months on the steam turbine. The CRON job performed a frequency sweep every 30 minutes. The collected files were retrieved using an SSH tunnel and transferring files to a local machine for processing.

4.2 Field Data Recorded for Various Frequencies

This section discusses the nature of the collected data on the field. As mentioned in Chapter 3, data collected for 1 second is trimmed down to merely 100 ms. Figures 4.1 to 4.7 were plotted using the data collected at Steam Turbine engine at the electrical power plant. The figures are created over 100 ms with the help of equation 3 i.e.,

$f(t) = \sum_{(n-1)\Delta t}^{n\Delta t} |i(t) + jq(t)|dt$, over 100 ms.

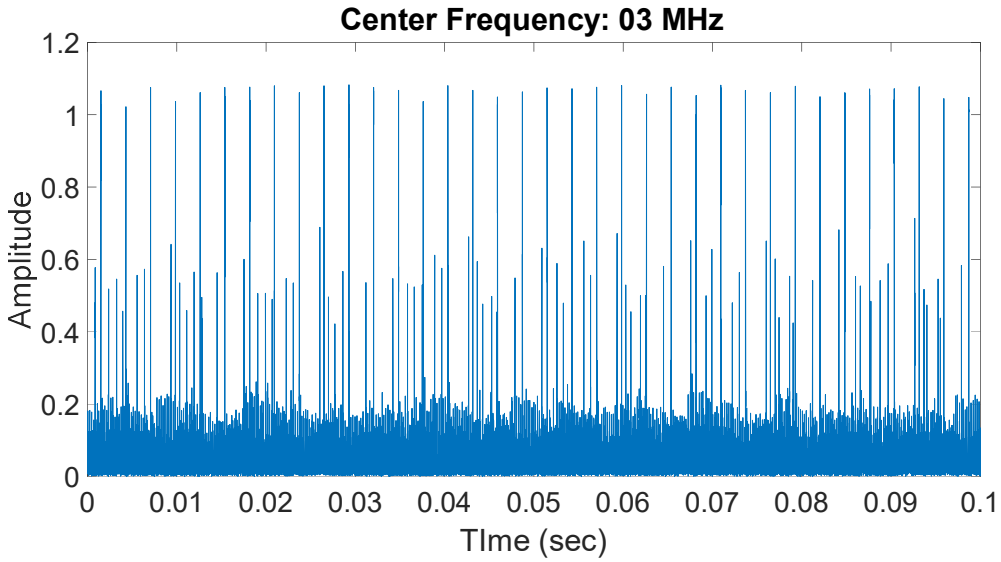

FIGURE 4.1: Radio tuned to 3 MHz.

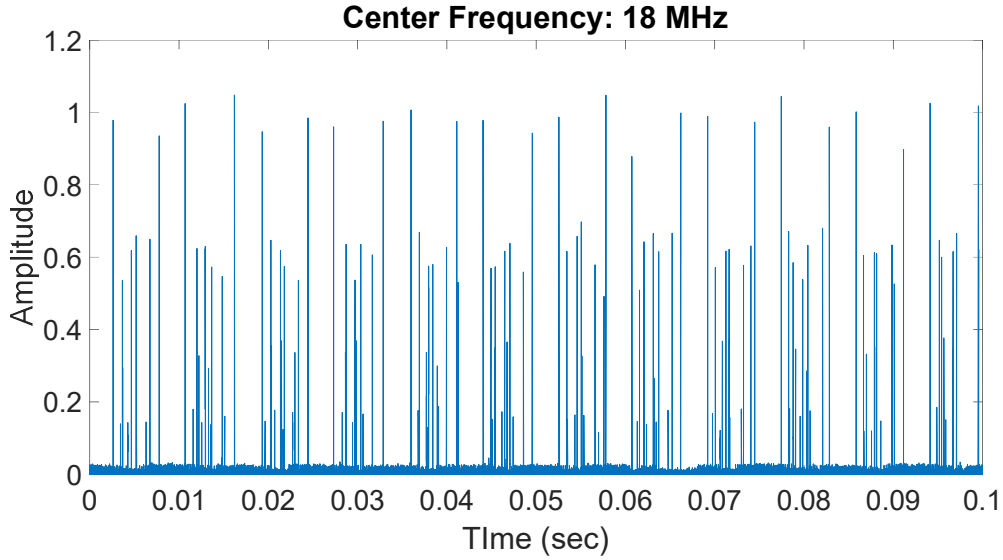

FIGURE 4.2: Radio tuned to 18 MHz.

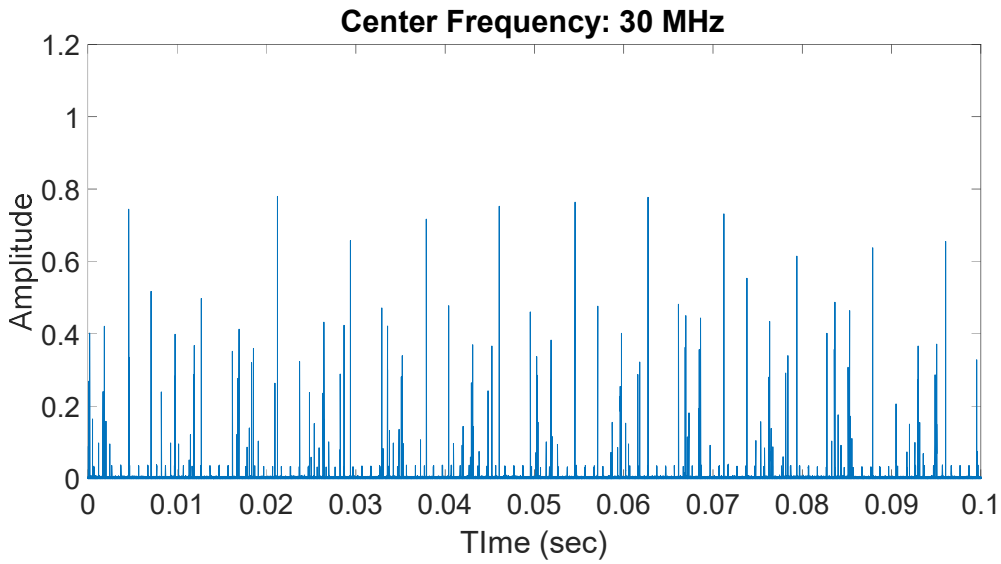

FIGURE 4.3: Radio tuned to 30 MHz.

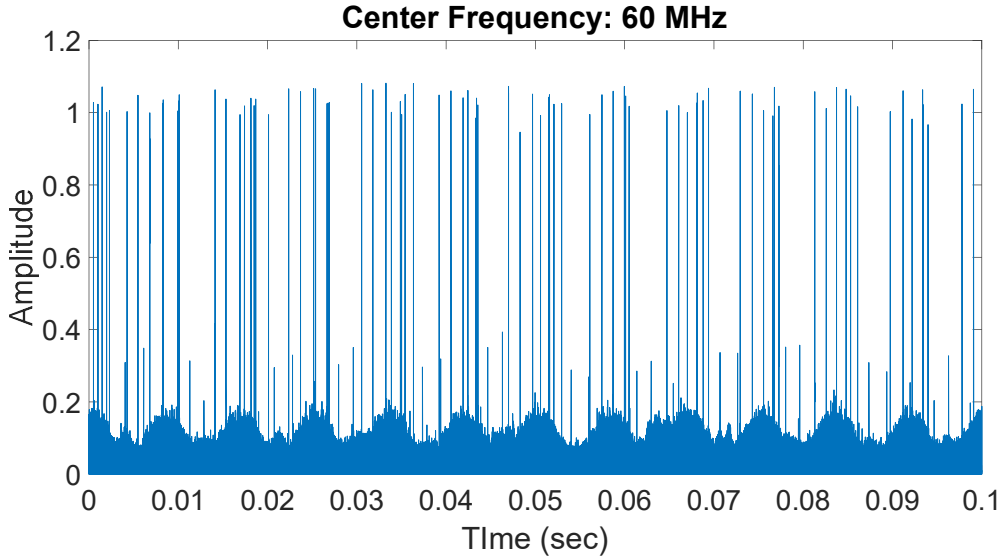

FIGURE 4.4: Radio tuned to 60 MHz.

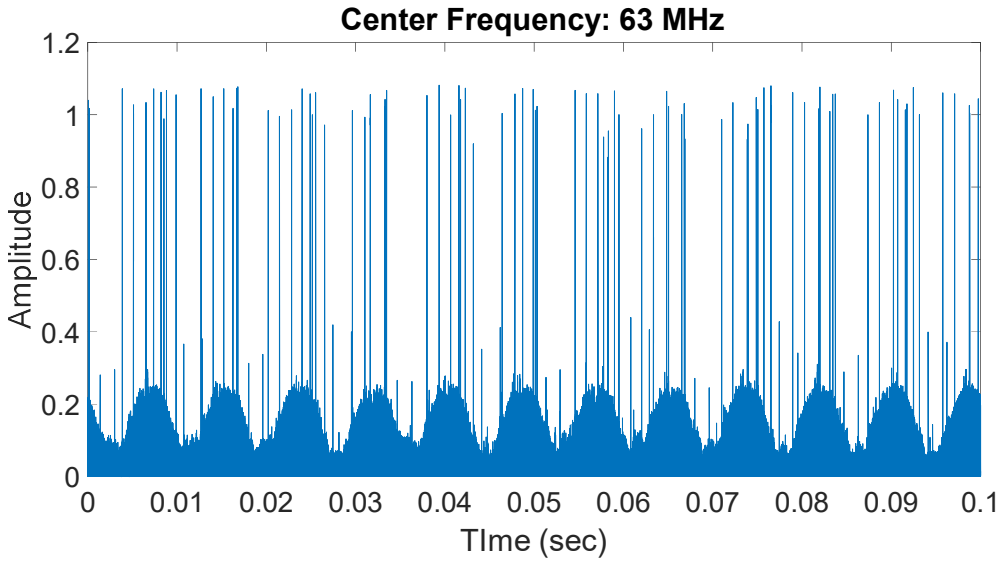

FIGURE 4.5: Radio tuned to 63 MHz.

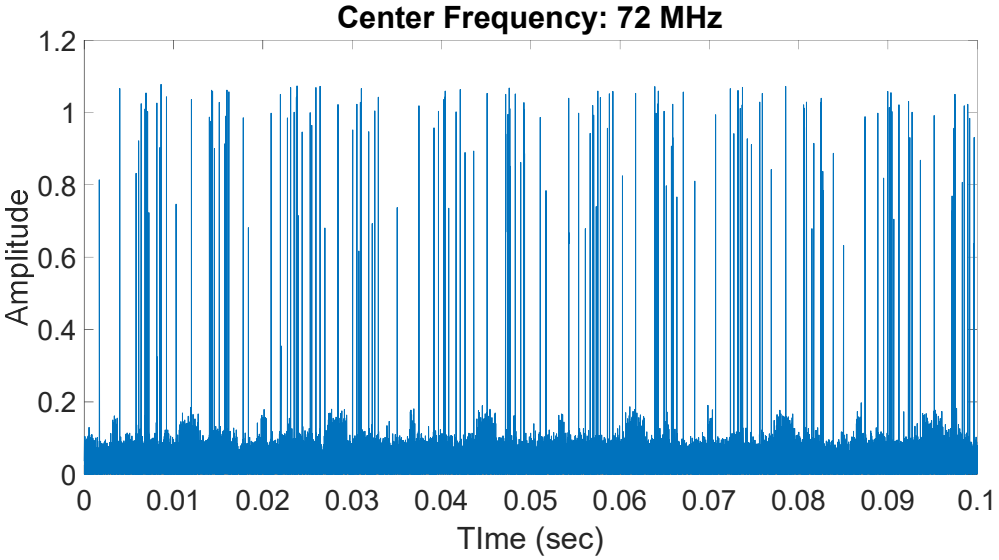

FIGURE 4.6: Radio tuned to 72 MHz.

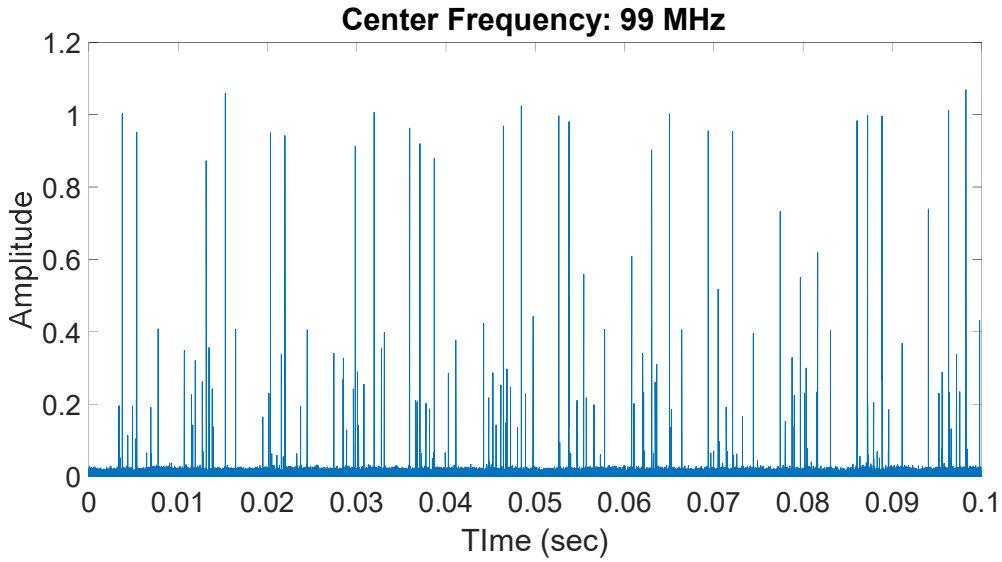

FIGURE 4.7: Radio tuned to 99 MHz.

Figures 4.8 to 4.14 were plotted using the data collected at Gas Turbine engine at the electrical power plant.

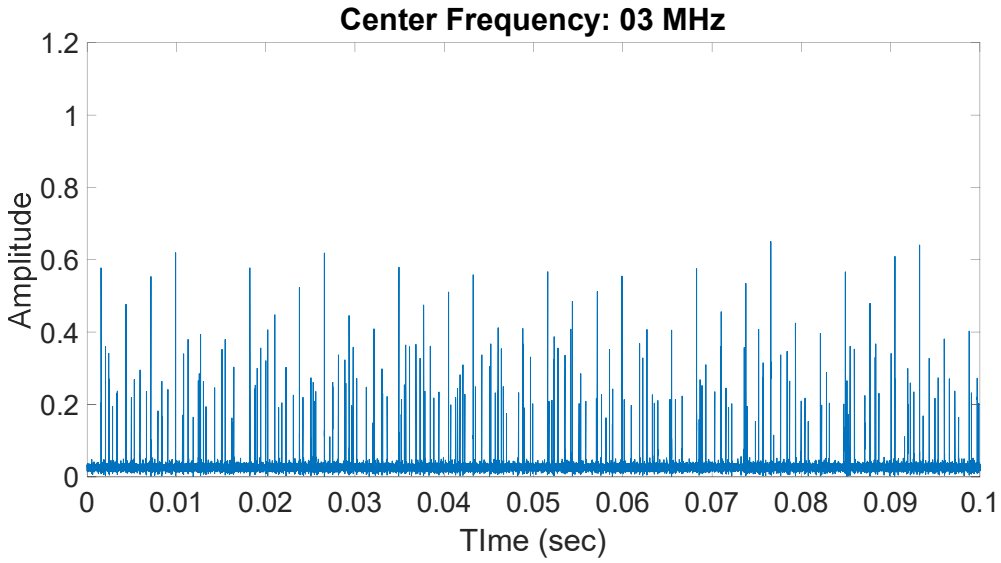

FIGURE 4.8: Radio tuned to 3 MHz.

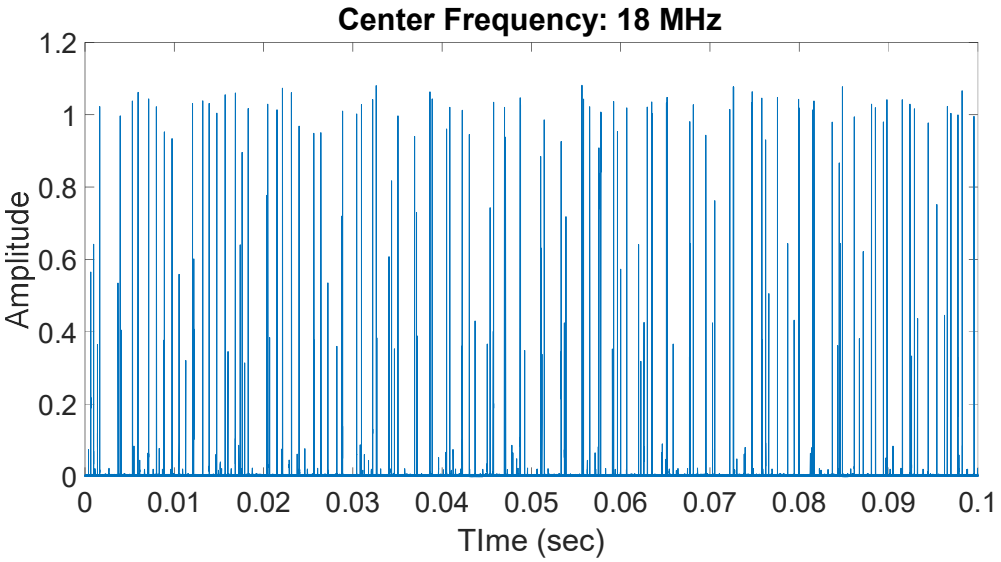

FIGURE 4.9: Radio tuned to 18 MHz.

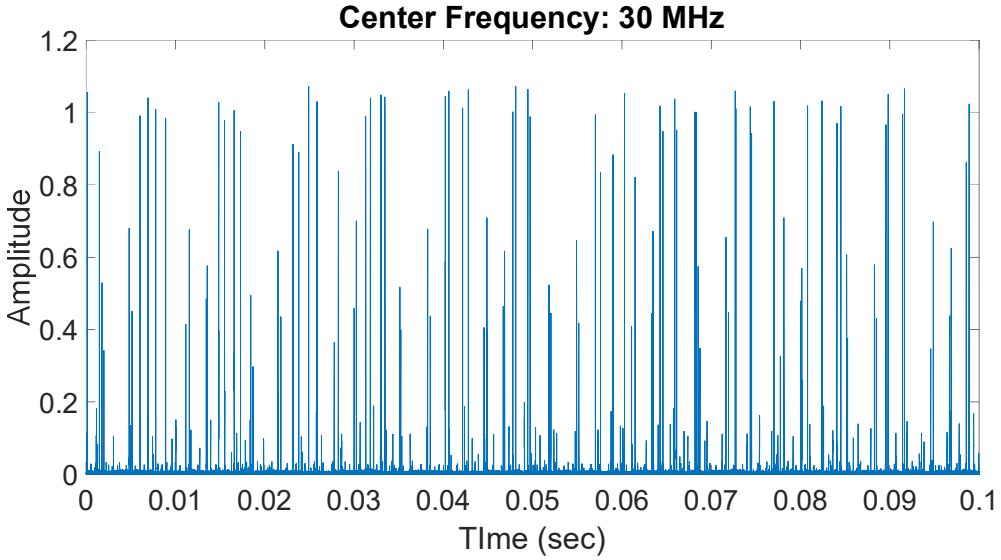

FIGURE 4.10: Radio tuned to 30 MHz.

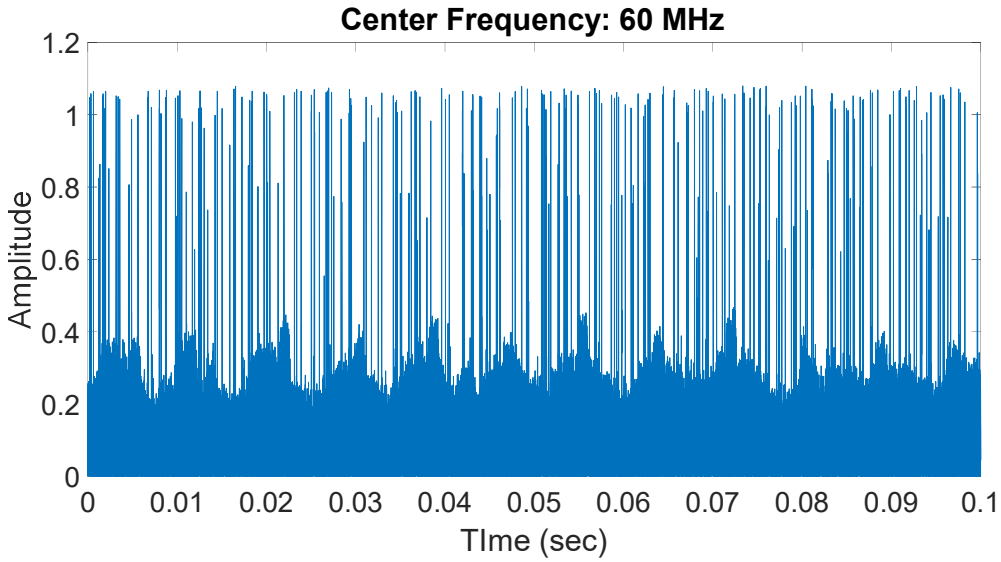

FIGURE 4.11: Radio tuned to 60 MHz.

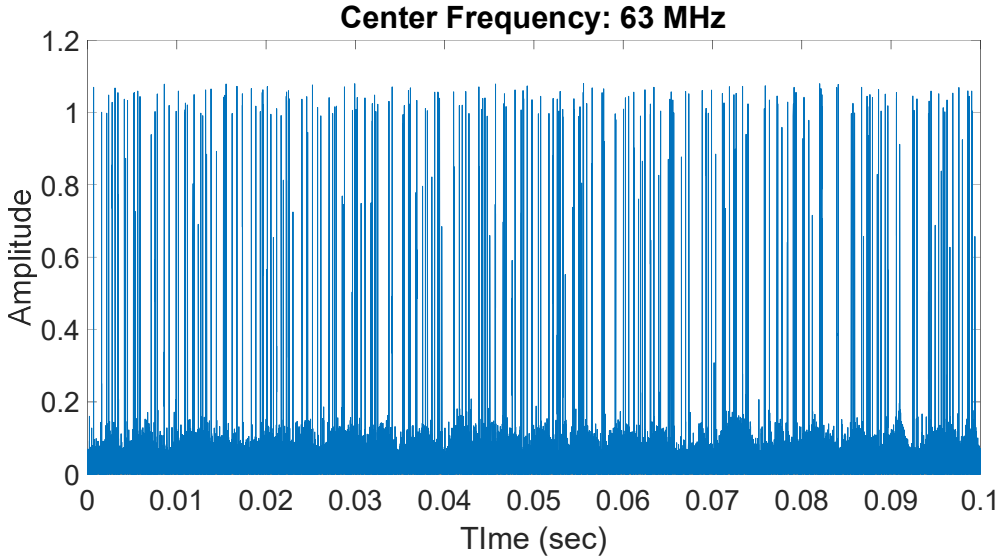

FIGURE 4.12: Radio tuned to 63 MHz.

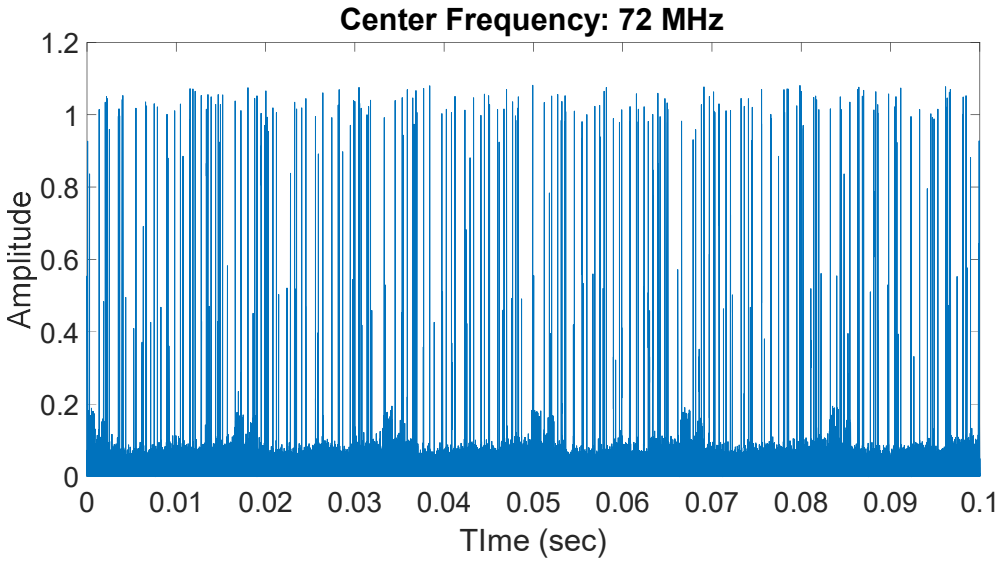

FIGURE 4.13: Radio tuned to 72 MHz.

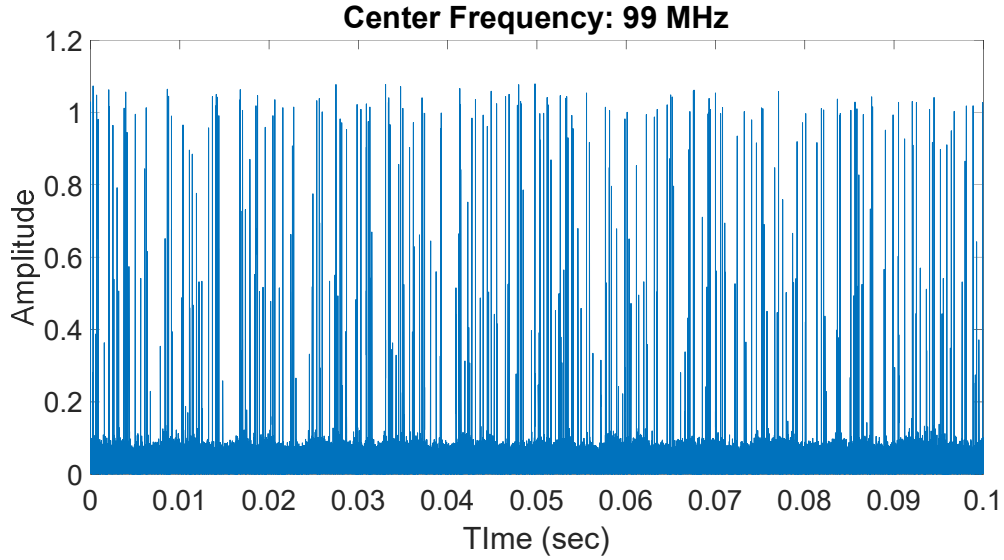

FIGURE 4.14: Radio tuned to 99 MHz.

From figure 2.3 that summarizes different faults associated to various frequency ranges[14] and figures 4.1 to 4.14, clearly show two observable issues from the nature of

data. Firstly, there are SCR patterns that are described to be at lower frequencies. We can notice the presence of pulses over the 60 Hz cycle especially at the lower frequencies. Secondly, above 60 Hz partial discharges are present, especially noticing the 60 MHz and 63 MHz – figures 4.4, 4.5, and 4.11. Thus, the raw time-series data collected by the proposed system is useful in identifying patterns essential for detecting various behaviors and partial discharge.

4.3 Developing Pattern Recognition Approach

Two important observations were made after collecting the data over couple of months and over various frequencies for both the turbines. Firstly, many signals repeat over each period of the 60Hz line frequency. Second observation, too much data is included when data is sampled at 9MHz to be able to perform any pattern recognition. Sampling at 9 MHz and collecting data for 100 ms, total of 1800000 data points are collected as I and Q values, which when converted to absolute value using equation 3, still sums up to 900000 points.

4.3.1 Feature Selection

Based on these two observations, three decisions were made for feature selection. First, use only data over one 60 Hz cycle, i.e. data over 16.66 ms. Sampling at 9 MHz, over 16.66 ms means only 150000 data points were taken under consideration.

Figure 4.15 shows data over just one 60 Hz cycle, when radio is tuned to 3 MHz.

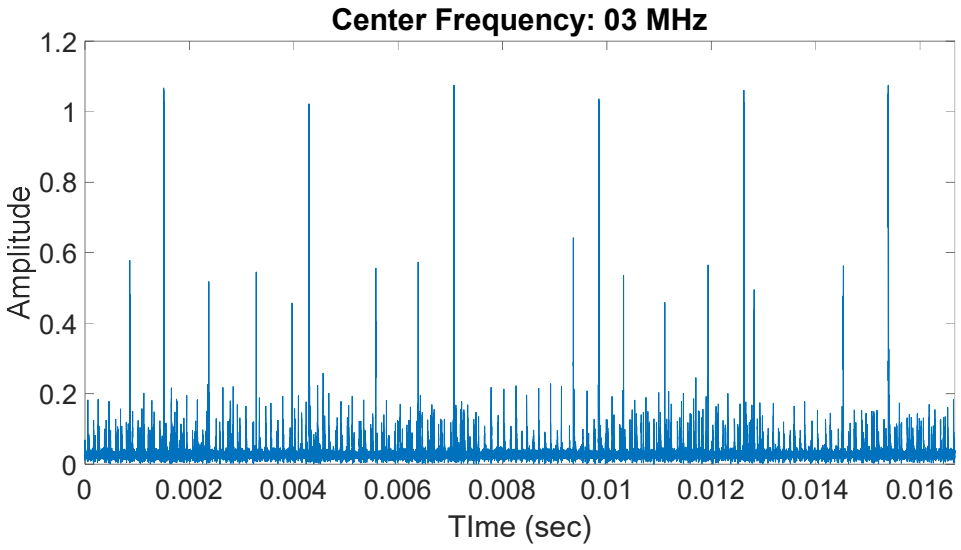

FIGURE 4.15: Radio tuned to 3 MHz, data within 16.66 ms.

As observed, many signals repeat over the 60 Hz frequency line, the cycle was divided into 360 windows, one window for each degree. For each of these windows, the maximum value of the window and the area under the curve was calculated and plotted for all the 360 windows - for the maximum of all windows and for the area under the curve for all windows. Figure 4.16 captures the notion of area under the curve and the maximum for 360 windows in over 150000 data points, over one 60 Hz cycle,

Area under the curve for a single window is calculated using equation 4, maximum value in a single window is calculated using equation 5

$$Area = \int_0^{\Delta t} |i(t) + jq(t)| dt \tag{4}$$

$$Maximum = \max_{t \,\epsilon [0, \Delta t]} |i(t) + jq(t)| \tag{5}$$

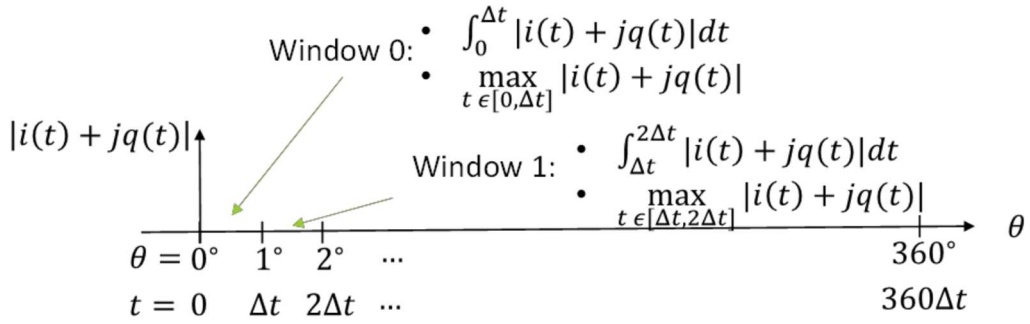

FIGURE 4.16: Area under the curve and maximum value for each of the 360 windows over one 60 Hz cycle.

4.3.2 Maximum Value and Area Under the Curve Over Various Frequencies

As discussed in 4.3.1, maximum and area under the curves were extracted for each window of the 360 windows over 60 Hz cycle. Figures 4.17 to 4.22 show the area under the curve calculated for 360 windows over 60 Hz cycle at various frequencies. These figures were created from data collected at the Steam Turbine engine at the utility partner's electrical power plant.

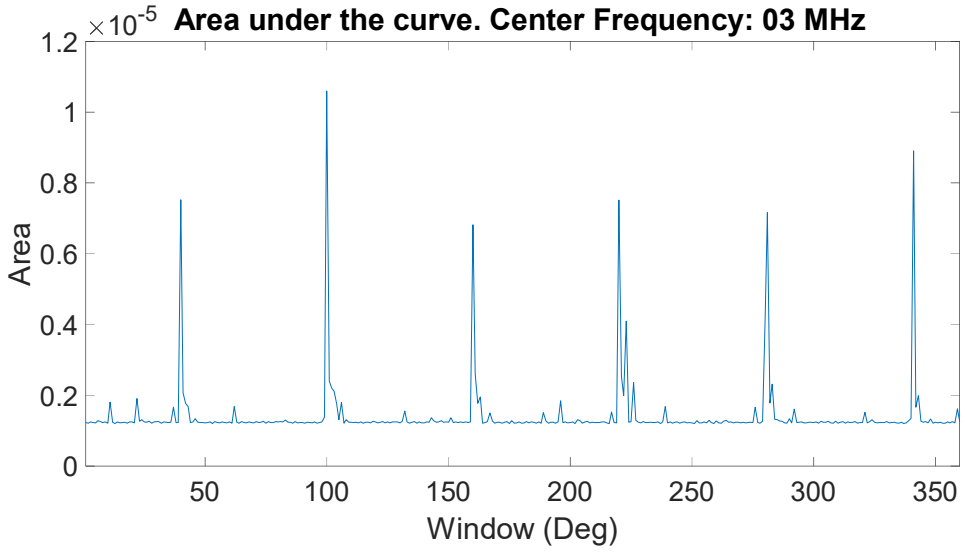

FIGURE 4.17: Area under the curve for each of the 360 windows over 60 Hz cycle. Radio tuned to 3 MHz.

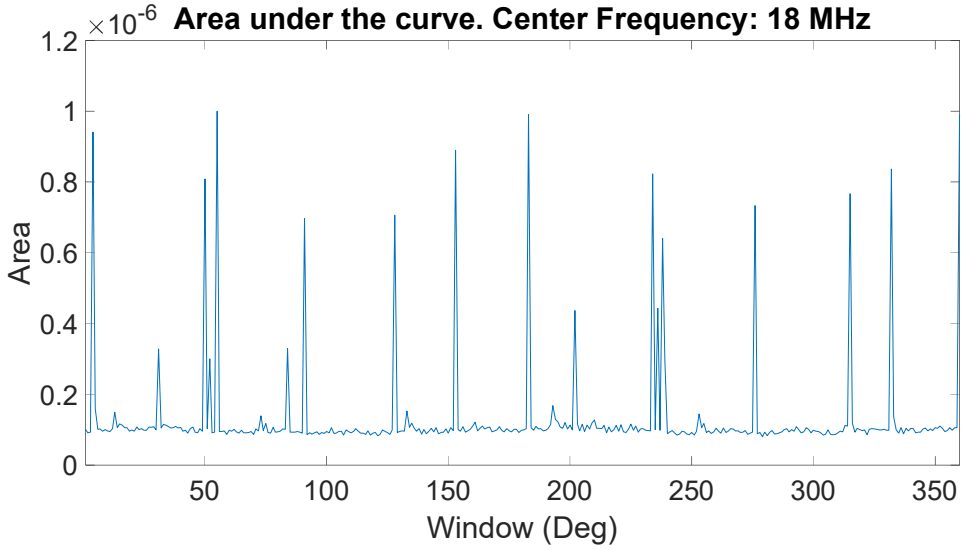

FIGURE 4.18: Area under the curve for each of the 360 windows over 60 Hz cycle. Radio tuned to 18 MHz.

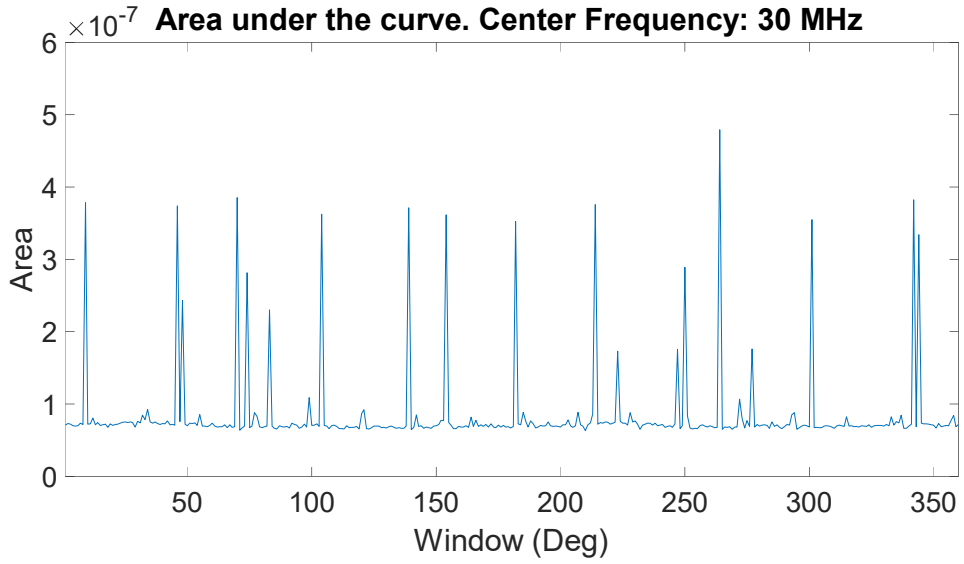

FIGURE 4.19: Area under the curve for each of the 360 windows over 60 Hz cycle. Radio tuned to 30 MHz.

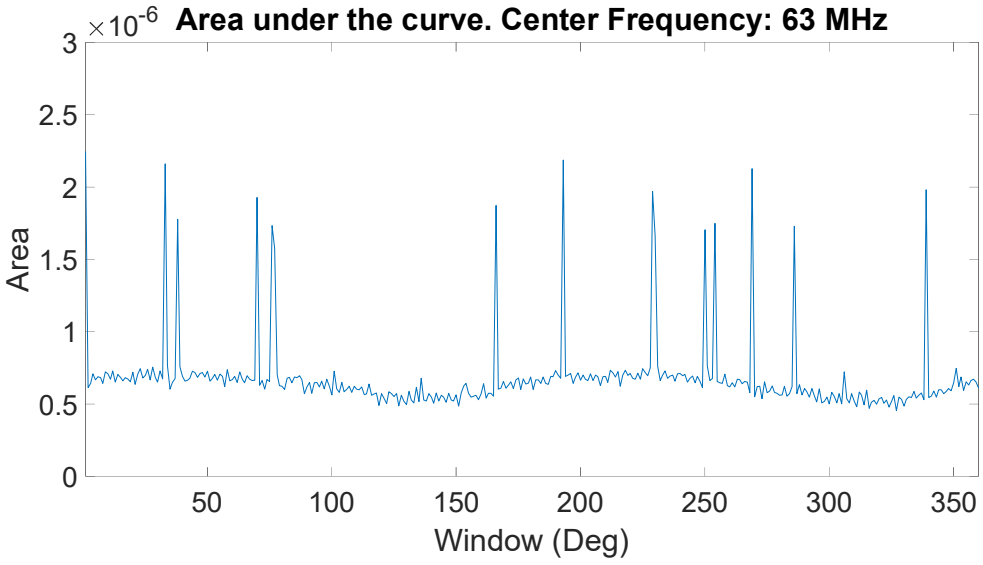

FIGURE 4.20: Area under the curve for each of the 360 windows over 60 Hz cycle. Radio tuned to 63 MHz.

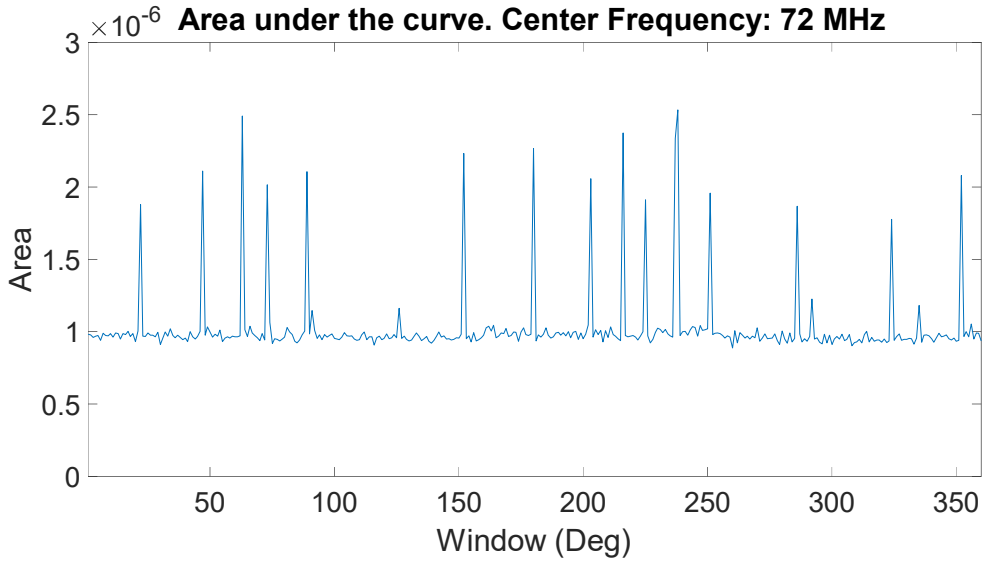

FIGURE 4.21: Area under the curve for each of the 360 windows over 60 Hz cycle. Radio tuned to 72 MHz.

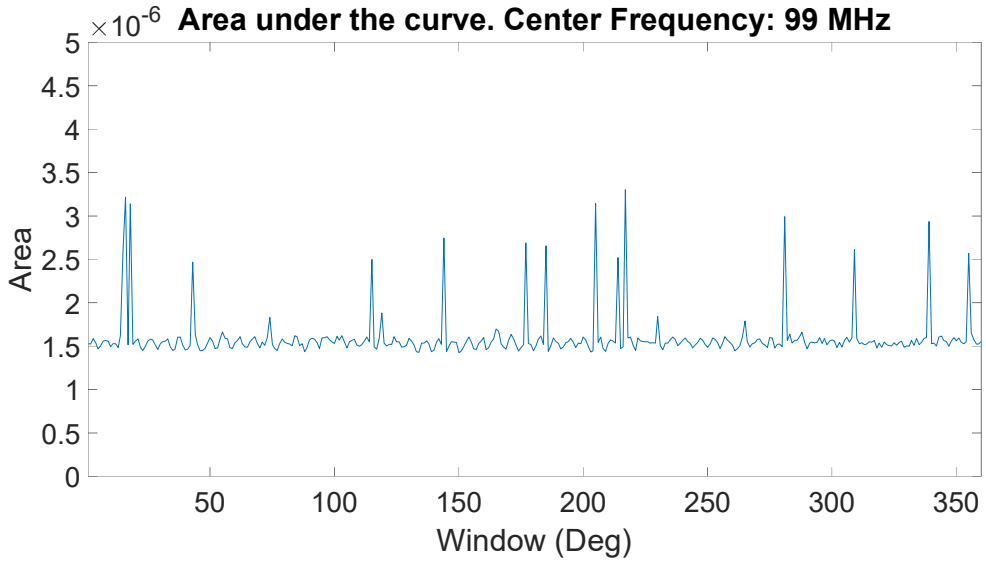

FIGURE 4.22: Area under the curve for each of the 360 windows over 60 Hz cycle. Radio tuned to 99 MHz.

Figures 4.23 to 4.28 show the maximum calculated for 360 windows over 60 Hz cycle at various frequencies, for the Steam Turbine engine at the utility partner's electrical power plant.

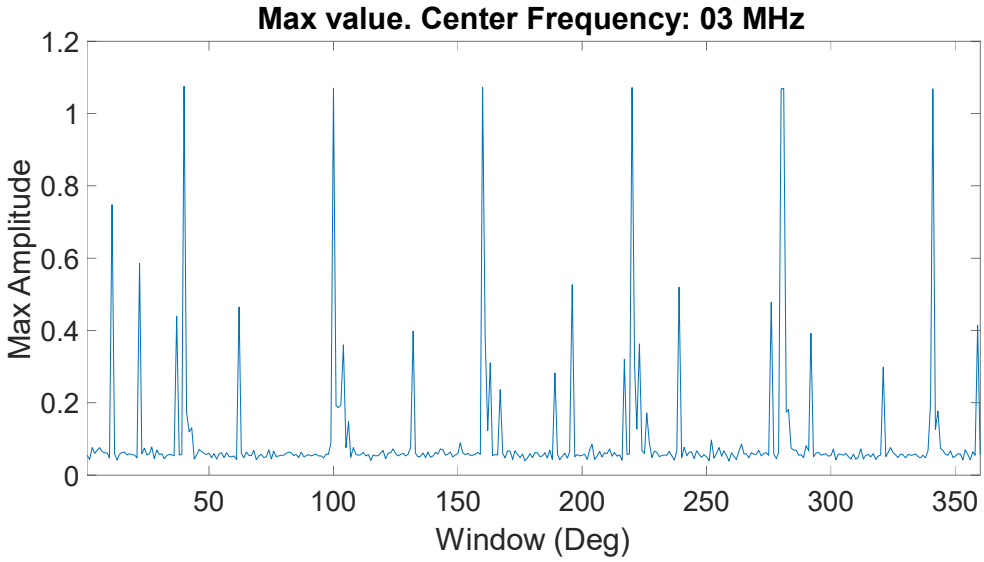

FIGURE 4.23: Maximum value for each of the 360 windows over 60 Hz cycle. Radio tuned to 3 MHz.

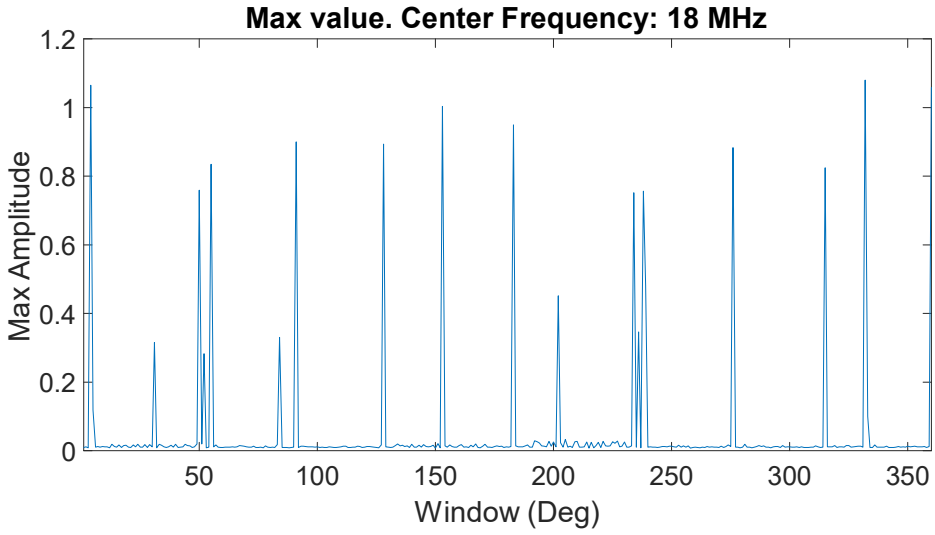

FIGURE 4.24: Maximum value for each of the 360 windows over 60 Hz cycle. Radio tuned to 18 MHz.

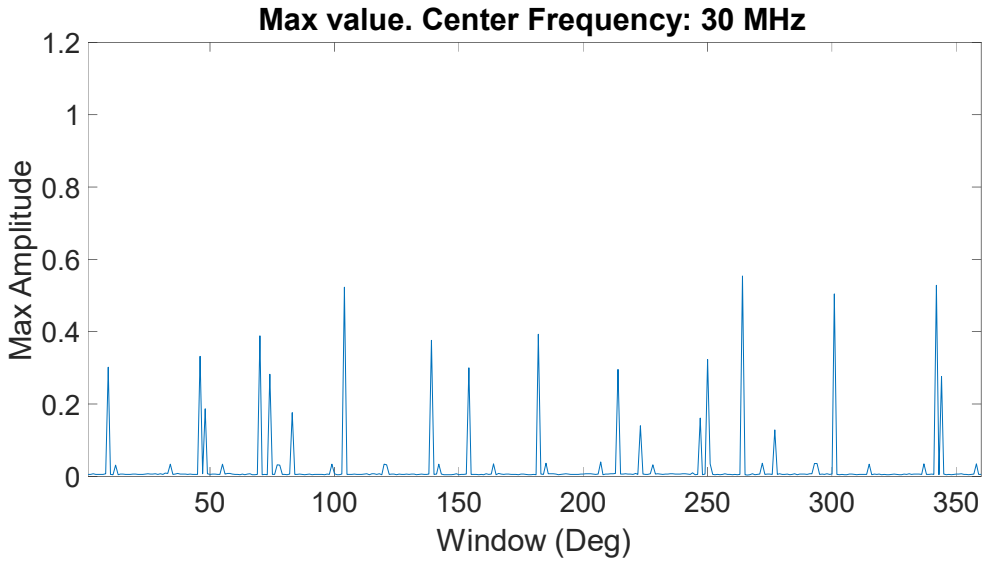

FIGURE 4.25: Maximum value for each of the 360 windows over 60 Hz cycle.

Radio tuned to 30 MHz.

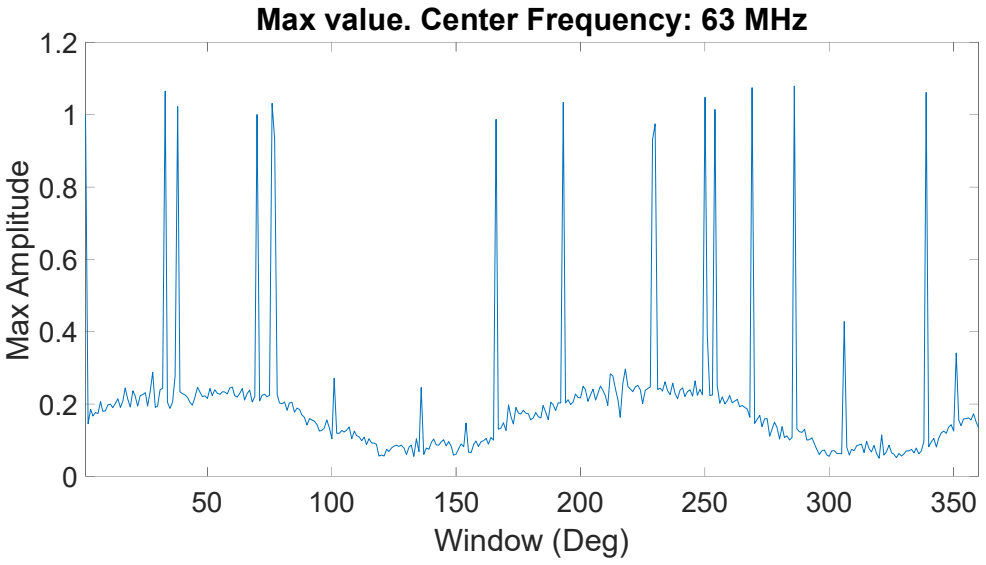

FIGURE 4.26: Maximum value for each of the 360 windows over 60 Hz cycle.

Radio tuned to 63 MHz.

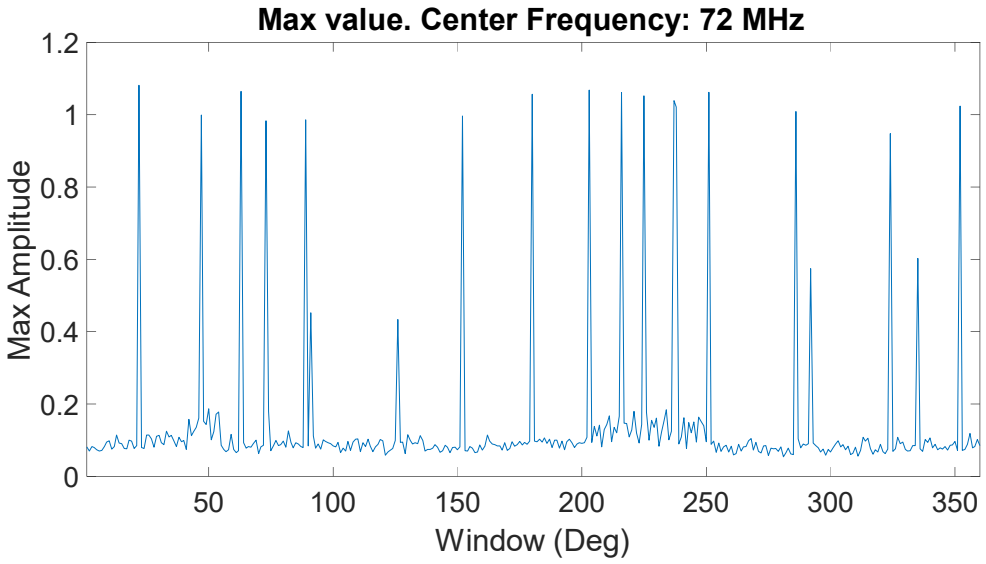

FIGURE 4.27: Maximum value for each of the 360 windows over 60 Hz cycle.

Radio tuned to 72 MHz.

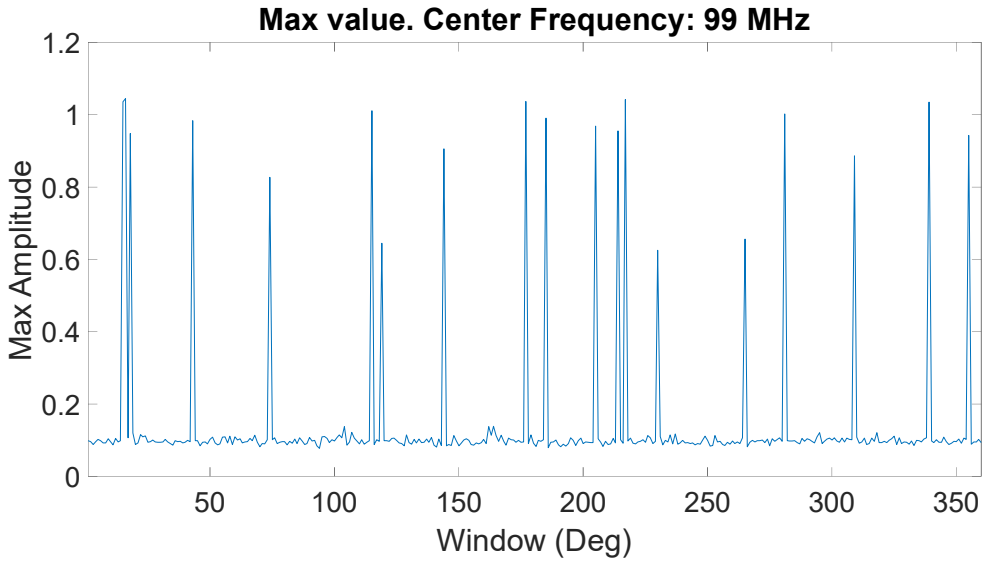

FIGURE 4.28: Maximum value for each of the 360 windows over 60 Hz cycle.

Radio tuned to 99 MHz.

CHAPTER 5: CONCLUSION AND FUTURE WORK

In this thesis, a new system was proposed for the detection of partial discharge in large machinery. The proposed system consists of three major components, namely a Radio Frequency Current Transformer, Software Defined Radio[28], and NVIDIA Jetson Nano[26]. The proposed system met the requirements necessary for replacing the current approach in EMSA which used a costly spectrum analyzer which is also a big piece of equipment, which also discards most of the data recorded by summarizing it into a single statistic value. The proposed system is small and costs just a fraction of that of the current system in place, hence easily deployable at multiple and remote locations. The proposed system also has the capability for being accessed remotely via the internet. SCR behaviors at lower frequencies and presence of partial discharges at higher frequencies were found using the proposed system deployed at the electrical power plant of the utility partner.

The next steps would be to deploy multiple systems at once at different power plants and perform testing for detecting partial discharges and remote monitoring. Along with pattern recognition performed on the data, since the data is a time-series data many machine learning models suitable for time-series data analysis such as the LSTM model or Convolutions Auto-Encoder model can be used for further additions to the pattern recognition and early fault detection techniques[20][21][22][23][24].

REFERENCES

[1] I. Culbert, J. Oliver, and W. Johnson, “Random wound motor failure investigation,” EPRI, Tech. Report 1000898, 2000.

[2] P. F. Albrecht, J.C. Appiarius, E. P. Cornell, D.W. Houghtaling, R.M. McCoy, E.L. Owens, “Assessment of the reliability of motors in utility applications,” *IEEE Transactions on Energy Conversion,* vol. EC-2, no 3, pp. 396-402, Sep. 1987.

[3] "Report of large motor reliability survey of industrial and commercial installation,” Part I and Part II, *IEEE Transactions on Industry Applications*, vol. 21, no. 4, pp. 853-872, Jul 1985.

[4] P. F. Albrecht, J. C. Appiarius, and D. K. Sharma, "Assessment of the reliability of motors in utility applications-Updated," *IEEE Transactions on Energy Conversion*, vol. EC-1, no 1 pp. 39-46, Mar 1986.

[5] “Condition monitoring solutions for motors and generators,” White Paper, ABB, 2012. [Online] https://library.e.abb.com/public/6b2d254d287d8d96c1257b2f003d8db2/Condition%20monitoring_LR.pdf

[6] S. Grubic, J. M. Aller, B. Lu, and T. G. Habetler, “A survey on testing and monitoring methods for stator insulation systems of low-voltage induction machines focusing on turn insulation problems,” *IEEE Transactions on Industrial Electronics,* vol. 55, no. 12, pp. 4127–4136, Dec. 2008.

[7] S. Nandi, H. A. Tolyat, and X. Li, “Condition monitoring and fault diagnosis of electric motors – A review,” *IEEE Transactions on Energy Conversion,* vol. 20, no. 4, Dec. 2005.

[8] M. Benbouzid, “A review of induction motors signature analysis as a medium for faults detection,” *IEEE Transactions on Industrial Electronics*, vol. 47, no. 5, pp. 984-993, Oct 2000.

[9] “SKF online motor analysis system – NetEP,” White Paper, SKF, 2012. [Online]: http://www.eis-inc.com/files/pdf/supplier_showcase_page_downloads/baker/NetEP%20brochure%20V6.pdf

[10] F. Filippetti, G. Franceschini, C. Tassoni, and P. Vas, “AI techniques in induction machines diagnosis including the speed ripple effect,” in *The Proceedings of the IEEE Industry Applications Society Annual Meeting*, San Diego, CA, Oct. 6–10, 1996, pp. 655–662

[11] S. Nandi, S. Ahmed, and H. A. Toliyat, “Detection of rotor slot and other eccentricity related harmonics in a three phase induction motor with different rotor cages,” *IEEE Transactions on Energy Conversion*, vol. 16, no. 3, pp. 253–260, Sep. 2001.

[12] S. Nandi, R. M. Bharadwaj, and H. A. Toliyat, “Performance analysis of a three phase induction motor under incipient mixed eccentricity condition,” *IEEE Transactions on Energy Conversion*, vol. 17, no. 3, pp. 392–399, Sep. 2002.

[13] D. Sinha, A. K. Verma and S. Kumar, "Software defined radio: Operation, challenges and possible solutions," in *2016 10th International Conference on Intelligent Systems and Control (ISCO)*, 2016.

[14] J. Stein, "Turbine-Generator Topics for Power Plant Engineers: Fundamentals of Electromagnetic Signature Analysis," EPRI, 2018.

[15] Y. Luo, Z. Li and H. Wang, "A review of online partial discharge measurement of large generators," *Energies,* 2017.

[16] X. Zhang, B. Pang, Y. Liu, S. Liu, P. Xu, Y. Li, Y. Liu, L. Qi and Q. Xie, "Review on Detection and Analysis of Partial Discharge along Power Cables," *Energies,* 2021.

[17] Y. Wang, "New Method for Measuring Statistical Distributions of Partial Discharge Pulses," *Journal of Research of the National Institute of Standards and Technology,* vol. 102, September - October 1997.

[18] A. Cavallini, G. C. Montanari and F. Puletti, "Partial Discharge Analysis and Asset Management: Experiences on Monitoring of Power Apparatus," 2006.

[19] M. Wu, H. Cao, J. Cao, H.-L. Nguyen, J. B. Gomes and S. P. Krishnaswamy, "An overview of state-of-the-art partial discharge analysis techniques for condition monitoring," *IEEE Electrical Insulation Magazine,* vol. 31, no. 6, pp. 22-35, November - December 2015.

[20] M. Florkowski, "Anomaly Detection, Trend Evolution, and Feature Extraction in Partial Discharge Patterns," Energies 2021, vol. 14, no. 13, 2021.

[21] N. Morette, L. C. Castro Heredia, T. Ditch, A. R. Mor and Y. Oussar, "Partial discharges and noise classification under HVDC using unsupervised learning," *Electrical Power and Energy Systems,* 2020.

[22] T. Ergen and S. S. Kozat, "Unsupervised Anomaly Detection With," *IEEE TRANSACTIONS ON NEURAL NETWORKS AND LEARNING SYSTEMS,* vol. 31, no. 8, August 2020.

[23] S. Barrios, D. Buldain, M. P. Comech, I. Gilbert and I. Orue, "Partial Discharge Classification Using Deep Learning," *Energies,* 2019.

[24] M. Florkowski, "Classification of Partial Discharge Images Using Deep Learning," *Energies,* 2020.

[25] "FCC:: Fischer Custom Communications," Fischer Custom Communications Inc., [Online]. Available: https://www.fischercc.com/.

[26] "NVIDIA Jetson Nano Developer Kit | NVIDIA Developer," NVIDIA, [Online]. Available: https://developer.nvidia.com/embedded/jetson-nano-developer-kit.

[27] “Hydrogenerator Failures – Results of the Survey,” CIGRE Study Committee SC11, Report EG11.02, 2003.

[28] "GNU Radio - The Free and Open Source Radio Ecosystem - GNU Radio," GNU Radio, [Online]. Available: https://www.gnuradio.org/.

[29] A. V. Oppenheim, A. S. WIllsky and S. H. Nawab, Signals And Systems, A. V. Oppenheim, Ed., Prentice Hall.

[30] "Guidelines to Perform Online Partial Discharge Measurements in Underground Power Cable," Rugged Monitoring, [Online]. Available: https://www.ruggedmonitoring.com/blog/guidelines-to-perform-online-partial-discharge-measurements-in-underground-power-cable/5e58add9cde096000141a77e.

[31] "RSP1A - SDRPlay," SDRPlay, [Online]. Available: https://www.sdrplay.com/rsp1a/.

[32] “Bently Nevada asset condition monitoring electric motor condition monitoring and protection application guide,” Application Note, General Electric, 2015. [Online] https://www.orbit-magazine.com/wp-content/uploads/2016/03/GEA32339-Elec-Motor-Cond-Monit-App-Guide_R3.pdf

[33] S. Zocholl, *AC Motor Protection*, Schweitzer Engineering Laboratories: Pullman, WA, 2003.